Cellular/Molecular

Ubiquitin Ligase RNF138 Promotes Episodic Ataxia Type 2-Associated Aberrant Degradation of Human $Ca_V2.1$ (P/Q-Type) Calcium Channels

Ssu-Ju Fu,[1] Chung-Jiuan Jeng,[5,6] Chia-Hao Ma,[2] Yi-Jheng Peng,[1] Chi-Ming Lee,[1] Ya-Ching Fang,[1] Yi-Ching Lee,[1] Sung-Chun Tang,[3] Meng-Chun Hu,[1] and Chih-Yung Tang[1,4]

[1]Department of Physiology and [4]Graduate Institute of Brain and Mind Sciences, College of Medicine, National Taiwan University, Taipei, 10051 Taiwan, [2]Department of Psychiatry and [3]Department of Neurology, National Taiwan University Hospital, Taipei, 10002 Taiwan, [5]Institute of Anatomy and Cell Biology, School of Medicine and [6]Brain Research Center, National Yang-Ming University, Taipei, 12212 Taiwan

Voltage-gated $Ca_V2.1$ channels comprise a pore-forming α_{1A} subunit with auxiliary $\alpha_2\delta$ and β subunits. $Ca_V2.1$ channels play an essential role in regulating synaptic signaling. Mutations in the human gene encoding the $Ca_V2.1$ subunit are associated with the cerebellar disease episodic ataxia type 2 (EA2). Several EA2-causing mutants exhibit impaired protein stability and exert dominant-negative suppression of $Ca_V2.1$ wild-type (WT) protein expression via aberrant proteasomal degradation. Here, we set out to delineate the protein degradation mechanism of human $Ca_V2.1$ subunit by identifying RNF138, an E3 ubiquitin ligase, as a novel $Ca_V2.1$-binding partner. In neurons, RNF138 and $Ca_V2.1$ coexist in the same protein complex and display notable subcellular colocalization at presynaptic and postsynaptic regions. Overexpression of RNF138 promotes polyubiquitination and accelerates protein turnover of $Ca_V2.1$. Disrupting endogenous RNF138 function with a mutant (RNF138-H36E) or shRNA infection significantly upregulates the $Ca_V2.1$ protein level and enhances $Ca_V2.1$ protein stability. Disrupting endogenous RNF138 function also effectively rescues the defective protein expression of EA2 mutants, as well as fully reversing EA2 mutant-induced excessive proteasomal degradation of $Ca_V2.1$ WT subunits. RNF138-H36E coexpression only partially restores the dominant-negative effect of EA2 mutants on $Ca_V2.1$ WT functional expression, which can be attributed to defective membrane trafficking of $Ca_V2.1$ WT in the presence of EA2 mutants. We propose that RNF138 plays a critical role in the homeostatic regulation of $Ca_V2.1$ protein level and functional expression and that RNF138 serves as the primary E3 ubiquitin ligase promoting EA2-associated aberrant degradation of human $Ca_V2.1$ subunits.

Key words: calcium channel; E3 ubiquitin ligase; episodic ataxia; membrane trafficking; protein degradation; ubiquitin–proteasome system

Significance Statement

Loss-of-function mutations in the human $Ca_V2.1$ subunit are linked to episodic ataxia type 2 (EA2), a dominantly inherited disease characterized by paroxysmal attacks of ataxia and nystagmus. EA2-causing mutants may exert dominant-negative effects on the $Ca_V2.1$ wild-type subunit via aberrant proteasomal degradation. The molecular nature of the $Ca_V2.1$ ubiquitin–proteasome degradation pathway is currently unknown. The present study reports the first identification of an E3 ubiquitin ligase for $Ca_V2.1$, RNF138. $Ca_V2.1$ protein stability is dynamically regulated by RNF138 and auxiliary $\alpha_2\delta$ and β subunits. We provide a proof of concept that protecting the human $Ca_V2.1$ subunit from excessive proteasomal degradation with specific interruption of endogenous RNF138 function may partially contribute to the future development of a novel therapeutic strategy for EA2 patients.

Introduction

Voltage-gated $Ca_V2.1$ (P/Q-type) Ca^{2+} channels are multisubunit membrane protein complexes comprising a principal voltage-sensing, pore-forming α_{1A} subunit in combination with auxiliary $\alpha_2\delta$ and β subunits (Catterall, 2000). $Ca_V2.1$ subunits are predominantly expressed in neurons and exhibit a subcellular local-

Received Oct. 2, 2016; revised Jan. 9, 2017; accepted Jan. 31, 2017.

Author contributions: C.-J.J., M.-C.H., and C.-Y.T. designed research; S.-J.F., C.-H.M., Y.-J.P., C.-M.L., Y.-C.F., Y.-C.L., S.-C.T., and M.-C.H. performed research; S.-J.F. and C.-Y.T. analyzed data; C.-J.J. and C.-Y.T. wrote the paper.

This work was supported by the Ministry of Science and Technology, Taiwan (Grant 105-2320-B-002-054-MY3 to C.-Y.T.). We thank Dr. Shi-Chuen Miaw for assistance with yeast two-hybrid screening.

The authors declare no competing financial interests.

Correspondence should be addressed to Dr. Chih-Yung Tang, Department of Physiology, College of Medicine, National Taiwan University, Taipei, 10051 Taiwan. E-mail: tang@ntu.edu.tw.

DOI:10.1523/JNEUROSCI.3070-16.2017

 0270-6474/17/372485-19$15.00/0

ization pattern involving axonal terminals and dendrosomatic regions (Catterall et al., 2005). $Ca_V2.1$ channels play a critical role in regulating neurotransmitter release from presynaptic terminals, as well as generating dendritic Ca^{2+} transients and setting the membrane excitability of dendrosomatic regions in postsynaptic neurons (Pietrobon, 2010; Catterall, 2011; Higley and Sabatini, 2012).

Episodic ataxia type 2 (EA2) is a rare, dominantly inherited cerebellar disease characterized by paroxysmal attacks of ataxia and nystagmus that are usually precipitated by emotional stress, physical exertion, or alcohol use; molecular genetic analyses in human patients have linked EA2 to mutations in the *CACNA1A* gene, which encodes the $Ca_V2.1$ subunit (Jen et al., 2004; Jen et al., 2007). To date, >20 mutations in $Ca_V2.1$ subunits were identified from familial or sporadic EA2 patients, most of which are nonsense (truncation) mutations, with the rest being missense mutations or aberrant splicing (Baloh, 2012; Nachbauer et al., 2014). So far, only a few missense EA2 mutations have been shown to generate functional human $Ca_V2.1$ channels, all displaying significantly smaller Ca^{2+} current amplitudes compared with their wild-type (WT) counterpart, which implies that virtually all EA2 mutations result in $Ca_V2.1$ proteins with loss-of-function phenotypes (Pietrobon, 2010; Rajakulendran et al., 2012).

The mechanisms underlying the EA2 dominant inheritance pattern appear to vary among different types of $Ca_V2.1$ mutations. Some of the truncated, nonfunctional EA2 mutants fail to exert discernible effects on $Ca_V2.1$ WT, implying a mechanistic role of haploinsufficiency in the pathophysiology of EA2 (Graves et al., 2008; Mantuano et al., 2010; Wan et al., 2011), which may result from nonsense-mediated mRNA decay triggered by the truncated $Ca_V2.1$ transcripts (Veneziano et al., 2011). In contrast, several lines of experimental evidence strongly suggest that some other EA2 nonsense and missense mutants may exert significant dominant-negative impacts on functional expression of WT channels (Jouvenceau et al., 2001; Page et al., 2004; Jeng et al., 2006; Raike et al., 2007; Jeng et al., 2008; Mezghrani et al., 2008; Page et al., 2010; Dahimene et al., 2016). Overall, the results from these studies suggest that misfolded EA2 mutants may exert their dominant-negative effects by disrupting the biosynthesis of $Ca_V2.1$ WT subunits via such mechanisms as unfolded protein response, endoplasmic reticulum (ER) retention, impaired membrane trafficking, or enhanced protein degradation.

Upon failing to pass the stringent scrutiny imposed by the ER quality control system, misfolded proteins are subject to ubiquitination and proteasomal degradation, a process known as ER-associated degradation (ERAD) (Vembar and Brodsky, 2008; Claessen et al., 2012). The notion that EA2-causing mutations may instigate ERAD of $Ca_V2.1$ subunits (Mezghrani et al., 2008) is very interesting in that it highlights the mechanistic role of the ubiquitin–proteasome system in the molecular pathophysiology of EA2. Moreover, given that neurotransmitter release probability is critically determined by the abundance of voltage-gated Ca^{2+} channels at active zones (Holderith et al., 2012; Hoppa et al., 2012; Sheng et al., 2012), the ubiquitin–proteasome system may control surface expression of $Ca_V2.1$ channels at presynaptic terminals and thereby contribute to homeostatic regulation of synaptic transmission. The molecular nature of $Ca_V2.1$ ubiquitin–proteasome degradation pathway is currently unknown. Here, we address this critical issue by identifying RNF138, a RING (Really Interesting New Gene) finger E3 ubiquitin ligase, as a novel binding partner of $Ca_V2.1$ subunits in neurons. Biochemical analyses reveal that RNF138 regulates the polyubiquitination and protein stability of $Ca_V2.1$. Moreover, we present evidence showing that RNF138 mediates aberrant protein degradation of EA2 mutants and contributes to the dominant-negative effects of EA2 mutants on $Ca_V2.1$ WT. Our data are consistent with the idea that RNF138 serves an E3 ubiquitin ligase for the homeostatic regulation of $Ca_V2.1$.

Materials and Methods

cDNA constructs. The cDNAs for Ca^{2+} channel α_1 subunits used in the study include human long-isoform α_{1A} ($Ca_V2.1$; AF004884; kindly provided by Dr. Joanna Jen, UCLA; Jen et al., 2001), human short-isoform α_{1A} ($Ca_V2.1$-Short; AF004883; kindly provided by Dr. Jörg Striessnig, University of Innsbruck; Wappl et al., 2002), rat α_{1C} ($Ca_V1.2$; M67515; kindly provided by Dr. Gerald Obermair, Medical University of Innsbruck; Obermair et al., 2004), and bovine α_{1B} ($Ca_V2.2$; AF173882; kindly provided by Dr. Aaron Fox, University of Chicago, and Dr. Chien-Yuan Pan, National Taiwan University; Cahill et al., 2000). Myc-tagged (C terminus) $Ca_V2.1$ constructs ($Ca_V2.1$-6myc) was created by subcloning $Ca_V2.1$ cDNA into a modified pcDNA3 vector (Invitrogen) with six repeats of Myc sequences right before the stop codon. The generation of GFP-tagged (N terminus) $Ca_V2.1$ was described previously (Jeng et al., 2008). cDNAs for human RNF128 and RNF138, as well as rat RNF138, were subcloned into the pcDNA3-Myc vector (Invitrogen). Other cDNAs include human Ca^{2+} channel auxiliary subunits $\alpha_2\delta$ and β_{4a} (NM_000722 and U95020; from Dr. Jen), bovine β_{1b} and β_{2a} (AF174415 and AF174417; from Dr. Fox), HA-tagged human wild-type and lysine-less ubiquitin (HA-Ub-WT and HA-Ub-K0; kindly provided by Dr. Chihiro Sasakawa, University of Tokyo). Where indicated, additional tagged or mutation constructs were created by introducing specific sequences into appropriate regions within the cDNAs using the QuikChange Site-Directed Mutagenesis Kit (Stratagene), followed by DNA sequence verification.

Yeast two-hybrid screening. The distal C-terminal region of human long-isoform α_{1A} ($Ca_V2.1$-C-ter; aa 2204–2510) was used as a bait to screen a rat brain cDNA library (OriGene) by using the DupLEX-A yeast two-hybrid system (OriGene). The cDNA for the $Ca_V2.1$-C-ter fragment was amplified by PCR and fused in-frame to the coding sequence for the DNA-binding protein LexA, which was in turn subcloned into the yeast expression plasmid pGilda and transformed (using the lithium acetate method) into the yeast strain EGY48 that contains the reporter gene LEU2 downstream of the LexA operator. To make certain that the LexA-$Ca_V2.1$-C-ter fusion protein was efficiently expressed in EGY48, transformed EGY48 yeast colonies were also cultured at 30°C in 4 ml of YPD rich medium harvested right before the colony density reached the OD_{600} value of 0.6, lysed in 20 μl of B-PER reagent (Pierce), and eventually subjected to immunoblotting analyses (Fig. 1*A*). The LexA-$Ca_V2.1$-C-ter-expressing EGY48 was then sequentially transformed with the reporter plasmid pSH18–34 (containing the LexA operator-lacZ fusion gene) and an activation-domain-fused cDNA library subcloned in the plasmid pJG4–5. After incubating at 30°C for 2–7 d, transformed yeast colonies growing on leucine dropout plates were scored positive for interacting proteins. Positive yeast colonies were further selected by β-galactosidase assay. Plasmid DNA extracted from yeast colonies was applied to transform the *E. coli* strain DH5α. Candidate cDNA clones were screened by PCR with pJG4–5-specific primers, followed by online (BLAST) and in-house sequence analyses. Of >490 candidate clones obtained with the bait, we identified 67 independent prey clones that were tested positive for $Ca_V2.1$ interactions. These 67 independent prey clones correspond to the partial or full amino acid sequences of ~30 distinct proteins.

Glutathione S-transferase (GST) pull-down assays. GST fusion proteins were produced and purified following the manufacturer's instructions (Stratagene). In brief, the cDNA fragments for human long-isoform α_{1A} N-terminal region ($Ca_V2.1$-N-ter; aa 1–99), transmembrane domains I and II linker ($Ca_V2.1$-I-II; aa 361–487), transmembrane domains II and III linker ($Ca_V2.1$-II-III; aa 715–1245), transmembrane domains III and IV linker ($Ca_V2.1$-III-IV; aa 1512–1567), proximal C-terminal region ($Ca_V2.1$-pC-ter; aa 1816–2203), and distal C-terminal region ($Ca_V2.1$-

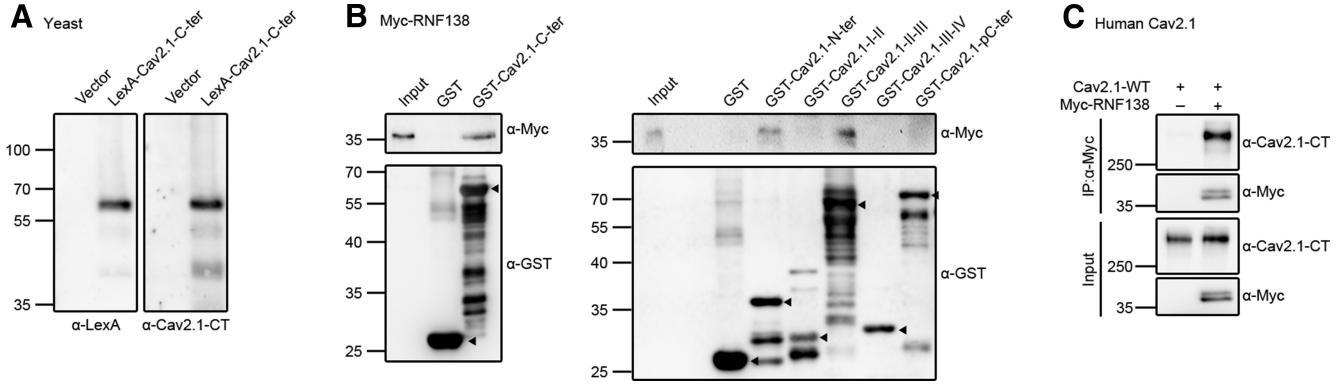

Figure 1. RNF138 is a novel binding partner of $Ca_V2.1$ subunit. ***A***, Bait construct for yeast two-hybrid screening comprises the pGilda plasmid containing the DNA-binding protein LexA fused in-frame with the distal C-terminal region ($Ca_V2.1$-C-ter) of human $Ca_V2.1$ long-isoform. Expression of the LexA-$Ca_V2.1$-C-ter fusion protein was only detected in EGY48 yeasts transformed with the bait-containing pGilda plasmid (LexA-$Ca_V2.1$-C-ter), but not with the pGilda vector per se (Vector). Protein samples (10 μl) were examined by immunoblotting with the anti-LexA (α-LexA) or anti-human $Ca_V2.1$ C-terminal (α-$Ca_V2.1$-CT) antibodies. Molecular weight marker (kDa) is labeled to the left. ***B***, GST pull-down assay. Left, Association of Myc-tagged rat RNF138 (Myc-RNF138) with the GST fusion protein comprising the $Ca_V2.1$-C-ter fragment (GST-$Ca_V2.1$-C-ter), but not with the GST protein per se. Right, Additional assays with GST-$Ca_V2.1$ fusion proteins comprising $Ca_V2.1$ N-terminal region ($Ca_V2.1$-N-ter), domains I and II linker ($Ca_V2.1$-I-II), domains II and III linker ($Ca_V2.1$-II-III), domains III and IV linker ($Ca_V2.1$-III-IV), or proximal C-terminal region ($Ca_V2.1$-pC-ter). Lysates from HEK293T cells overexpressing Myc-RNF138 were used for GST pull-down assay, followed by immunoblotting with the anti-Myc antibody (α-Myc). GST and GST-$Ca_V2.1$ fusion proteins were detected with the anti-GST antibody (α-GST). Input represents ~1% of total cell lysate volume. Arrowheads denote the location of GST or GST-$Ca_V2.1$ fusion protein bands. ***C***, Coimmunoprecipitation of Myc-RNF138 with the human $Ca_V2.1$ long-isoform ($Ca_V2.1$-WT). Coexpression with the Myc vector was used as the control. HEK293T cell lysates were immunoprecipitated (IP) with α-Myc, followed by immunoblotting with α-Myc or the anti-human $Ca_V2.1$ C-terminal antibody (α-$Ca_V2.1$-CT). The apparent molecular weight of human $Ca_V2.1$ long-isoform is ~280–290 kDa. Corresponding expression levels of human $Ca_V2.1$ and Myc-RNF138 in the lysates are shown in the "input" lane. Hereafter, input represents ~10% of the total protein used for immunoprecipitation.

C-ter; aa 2204–2510) were subcloned into the pGEX vector (GE Healthcare) and expressed in the *E. coli* strain BL21. Bacterial cultures were grown at 30°C, induced with 0.1 mM isopropyl-β-D-thiogalactopyranoside, and then harvested by centrifugation at 8000 × *g* for 10 min at 4°C. Cell pellets were resuspended in B-PER reagent (Pierce) containing 1 mM phenylmethylsulfonyl fluoride (PMSF) and a protease inhibitor mixture (Roche Applied Science). The lysates were clarified by centrifugation at 15,000 × *g* for 15 min, and glutathione-agarose beads (Sigma-Aldrich) were used to bind the GST fusion proteins from the supernatant. GST protein-coated beads (4–8 μg) were incubated with precleared cell lysates at 4°C overnight. The bead–protein complexes were then washed with buffer A containing the following (in mM): 100 NaCl, 4 KCl, 2.5 EDTA, 20 $NaHCO_3$, 20 Tris-HCl, pH 7.5, 1 PMSF, 1 Na_3VO_4, 1 NaF, and 1 β-glycerophosphate with and without 1% Triton X-100 and the proteins were eluted by boiling for 5 min in the Laemmli sample buffer.

Cell culture and DNA transfection. Human embryonic kidney (HEK) 293T cells (RRID:CVCL_0063) or neuroblastoma NT2 cells (RRID:CVCL_0034; kindly provided by Dr. Thai-Yen Ling, National Taiwan University) were grown in DMEM supplemented with 2 mM glutamine, 10% heat-inactivated fetal bovine serum (Hyclone), 100 units/ml penicillin, and 50 μg/ml streptomycin and maintained at 37°C in a humidified incubator with 95% air and 5% CO_2. Transient transfection was performed by using the Lipofectamine 2000 (LF2000) reagent (Invitrogen). Briefly, cells were plated onto six- or 12-well plates (for biochemical experiments) or poly-D-lysine-coated coverslips in 24-well plates (for electrophysiological recordings) 24 h before transfection. Various expression constructs were incubated with LF2000 reagent for 20 min at room temperature and DNA-Lipofectamine diluted in Opti-MEM (Invitrogen) was applied to culture wells. After 6 h of incubation at 37°C, the medium was changed and the culture cells were maintained in a humidified 5% CO_2 incubator at 37°C for 24–48 h before being used for biochemical or electrophysiological experiments. For immunoprecipitation and ubiquitination experiments, transfected HEK293T cells were incubated in the presence of 10 μM MG132 (Sigma-Aldrich) for 24 h.

Immunoblotting. Transfected cells were washed twice with ice-cold PBS containing the following (in mM): 136 NaCl, 2.5 KCl, 1.5 KH_2PO_4, and 6.5 Na_2HPO_4, pH 7.4, centrifuged, and resuspended in a lysis buffer containing the following (in mM): 150 NaCl, 5 EDTA, and 50 Tris-HCl, pH 7.6, 1% Triton X-100 containing a protease inhibitor mixture. After adding the Laemmli sample buffer to the lysates, samples were sonicated on ice (3 times for 5 s each) and heated at 70°C for 5 min. Samples were then separated by 7.5–10% SDS-PAGE, electrophoretically transferred to nitrocellulose membranes, and detected using mouse anti-β-actin (1:5000; Millipore catalog #MAB1501, RRID:AB_2223041), rabbit anti-human $Ca_V2.1$-CT [1:2500; the C-terminal region (aa 2369–2473) of human $Ca_V2.1$ long-isoform], rabbit anti-human $Ca_V2.1$-(II-III) [1:2500; the linker region (aa 888–904) between transmembrane domains II and III of human $Ca_V2.1$], rabbit anti-rat $Ca_V2.1$ (1:200; Alomone Laboratories catalog #ACC-001, RRID:AB_2039764), rabbit anti-Flag (1:5000; Sigma-Aldrich catalog #F7425, RRID:AB_439687), rabbit anti-GAPDH (1:8000; GeneTex catalog #GTX100118, RRID:AB_1080976), rabbit anti-GFP (1:2500, Abcam catalog #ab290, RRID:AB_303395), mouse anti-GST tag (1:5000; Eno-Gene catalog #E12-007), rat anti-HA (1:5000; Roche catalog #11867423001, RRID:AB_10094468), rabbit anti-LexA (1:5000; Millipore catalog #06-719, RRID:AB_310223), mouse anti-Myc (1:5000; clone 9E10), mouse anti-postsynaptic density-95 (anti-PSD-95, 1:5000; UC Davis/NIH NeuroMab Facility catalog #75-028, RRID:AB_2307331), rabbit anti-RNF138 (1:200; Abcam catalog #ab92730, RRID:AB_2238719), mouse anti-synaptophysin (1:5000; clone 6D5AC4), rabbit anti-α-tubulin (1:5000; GeneTex catalog #GTX112141, RRID:AB_10722892), or mouse anti-ubiquitin (1:1000; Enzo Life Sciences catalog #BML-PW8810, RRID:AB_10541840) antibodies. Blots were then exposed to horseradish-peroxidase-conjugated goat anti-mouse IgG (1:5000; Jackson ImmunoResearch catalog #115-035-003, RRID:AB_10015289), goat anti-rabbit IgG (1:5000; Jackson ImmunoResearch catalog #111-035-003, RRID:AB_2313567), or goat anti-rat IgG (1:5000; Santa Cruz Biotechnology catalog #sc-2032, RRID:AB_631755) and revealed by an enhanced chemiluminescence detection system (Thermo Scientific). Results shown are representative of at least three independent experiments. Densitometric scans of immunoblots were quantified with ImageJ (RRID:SCR_003070).

Immunoprecipitation. Cells were solubilized in ice-cold lysis buffer containing the protease inhibitor mixture. Insolubilized materials were removed by centrifugation. Solubilized HEK293T cell lysates or brain homogenates were precleared with protein A/G Sepharose beads (GE Healthcare Biosciences) for 1 h at 4°C and then incubated for 16 h at 4°C with protein A/G Sepharose beads precoated with appropriate antibodies. Beads were gently spun down and washed twice in a wash buffer containing the following (in mM): 100 NaCl, 4 KCl, 2.5 EDTA, 20 $NaHCO_3$, and 20 Tris-HCl, pH 7.5, supplemented with 0.1% Triton X-100 and then twice with the wash buffer. The immune complexes were

eluted from the beads by heating at 70°C for 5 min in the Laemmli sample buffer.

Rat brain lysates and subcellular fractionation. All animal procedures are in accordance with the *Guidelines for the Care and Use of Mammals in Neuroscience and Behavioral Research* (National Research Council, 2003) and approved by the Institutional Animal Care and Use Committee of the College of Medicine, National Taiwan University.

Forebrains from adult Sprague Dawley rats (RRID:RGD_5508397) were homogenized with a motor driven glass-Teflon homogenizer in ice-cold dissociation buffer containing the following (in mM): 320 sucrose, 1 $MgCl_2$, 0.5 $CaCl_2$, 1 $NaHCO_3$, 1 PMSF, and 1 mg/L leupeptin) and the cell debris was removed by centrifugation at 1400 × *g* for 10 min. The supernatant was saved and the pellet was resuspended by homogenization in ice-cold dissociation buffer and pelleted again. The remaining pellet was discarded and the combined supernatants were pelleted (13,800 × *g* for 10 min) again. The final pellet was resuspended in buffer A supplemented with 1% Triton X-100 and protease inhibitor mixture.

For subcellular fractionation, rat forebrains were homogenized in buffer H1 containing the following (in mM): 320 sucrose, 1 $NaHCO_3$, 0.5 $CaCl_2$, and 0.1 PMSF, along with protease inhibitor mixture, and centrifuged at 1400 × *g* to remove nuclei and other large debris (P1). The S1 fraction was subject to centrifugation at 13,800 × *g* to obtain the crude synaptosome fraction (P2). The pellet was resuspended in buffer H2 containing the following (in mM): 0.32 M sucrose and 1 mM $NaHCO_3$, and layered onto the top of the discontinuous sucrose density gradient by using 0.85, 1.0, and 1.2 M sucrose layers. The gradient was centrifuged at 65,000 × *g* for 2 h in a Beckman Instruments SW-28 rotor and the synaptosomal fraction (SPM) was recovered from the 1.0–1.2 M sucrose interface. The synaptosomal fraction was extracted in ice-cold 0.5% Triton X-100/50 mM Tris-HCl, pH 7.9, for 15 min and centrifuged at 32,000 × *g* for 45 min to obtain the PSD I pellet. The pellet was resuspended and further extracted a second time with 0.5% Triton X-100/50 mM Tris-HCl, pH 7.9, followed by centrifugation at 200,000 × *g* for 45 min to obtain the PSD II pellet. Protein concentration was determined by the BCA protein assay kit (Thermo Scientific). For immunoblotting, 40 μg (H, S1, P2, and SPM) or 20 μg (SPM, PSD I, and PSD II) of proteins were used.

Cortical neuron cultures. Dissociated cortical cultures were prepared using a previously described protocol (Banker and Goslin, 1998) with a minor modification. In brief, the forebrains of embryonic day 18 embryos isolated from pregnant rats were removed and placed in Hank's balanced salt solution containing 10 mM HEPES, pH 7.4, and 1 mM sodium pyruvate. The cortex was dissected out and dissociated by incubation with 0.25% trypsin solution. The dissociated cells were plated on coverslips at a density of ~160 and 800 cells/mm^2 for immunofluorescence and immunoblotting, respectively. Coverslips were precoated with poly-D-lysine (1 mg/ml; Sigma-Aldrich) and laminin (15 μg/ml; Sigma-Aldrich). Cultures were maintained in Neurobasal medium supplemented with B27 (2%) and Glutamax I (0.5 mM; Invitrogen).

Immunofluorescence. Coverslips containing cortical neurons were rinsed in PBS and then fixed with methanol (at 4°C) or 4% paraformaldehyde (at room temperature) in PBS for 20 min. Cells were then permeabilized and blocked with a blocking buffer [5% normal goat serum in 20 mM phosphate buffer, pH 7.4, 0.1% (v/v) Triton X-100, and 0.45 M NaCl] for 60 min at 4°C. Appropriate dilutions of primary antibodies were applied in the blocking buffer overnight at 4°C. Immunoreactivities were visualized with goat-anti-mouse antibodies conjugated to Alexa Fluor 568 (1:200; Invitrogen catalog #A11004, RRID:AB_141371) or with goat anti-rabbit antibodies conjugated to Alexa Fluor 488 (1:200; Invitrogen catalog #A11008, RRID:AB_143165). The fluorescence images were viewed and acquired with a Leica TCS SP5 laser-scanning confocal microscope. To quantify the number of protein clusters per fixed length of neurites in cultured cortical neurons, built-in "set scale" and "freehand tool" functions of ImageJ were used to trace multiple 100 μm neurite segments, followed by counting the $Ca_V2.1$/RNF138/synaptophysin/PSD-95 puncta within each 100 μm neurite segment. Colocalization of $Ca_V2.1$/RNF138 (green punctate pixels) with synaptophysin/PSD-95 (red punctate pixels) puncta was expressed as the fraction of puncta identified as both green and red punctate pixels within each 100 μm neurite segment.

RNA interference. Lentivirus-based shRNA constructs (subcloned into the pLKO.1 vector) targeting specific human RNF138 (RNF138-1: 5′-CCTAGCCAGATTACCAGAAAT-3′; RNF138-2: 5′-GCTAGATGAAGAAACCCAATA-3′) and $Ca_V2.1$ (5′-CCCTCAGGTTATTGCGTATTT-3′) sequences were purchased from the National RNAi Core Facility, Taiwan. The shRNA for GFP (5′-GACCACCCTGACCTACGGCGT-3′) was used as a control. Recombinant lentivirus was generated by transfecting HEK293T cells with the packaging plasmid pCMV-ΔR8.91, the envelope plasmid pMD.G, and shRNA expressing constructs. The virus-containing supernatant was harvested and concentrated by ultracentrifugation to yield the viral stock, which in turn was supplemented with 8 μg/ml polybrene for infection of HEK293T, NT2, or cortical cells. The infected cells were selected by 5 μg/ml puromycin and subsequently transfected with the cDNA for $Ca_V2.1$. For suppressing endogenous $Ca_V2.1$/RNF138 in cultured cortical neurons, 9 d *in vitro* (DIV9) neurons were infected with shRNA. After puromycin selection, infected DIV12 neurons were subject to immunoblotting analyses.

RT-PCR. RNA was extracted from HEK293T cells or cortical neurons with TRIzol (Sigma-Aldrich), followed by phenol/chloroform separation. To eliminate potential plasmid DNA contamination in the RNA prepared from HEK293T cells transfected with $Ca_V2.1$, we performed DNase I (Promega) treatment as a control experiment. RNA was reverse transcribed into cDNA using High-Capacity cDNA Reverse Transcription Kit with RNase Inhibitor (Thermo Scientific). The reaction mixture was incubated at 25°C and 37°C for 10 min and 120 min, respectively, followed by heating to 85°C for 5 min. PCR amplification with *Taq* polymerase (Bioman) was performed as follows: 95°C for 5 min; nonsaturating 20 (HEK293T cells) or 25 (cortical neurons) cycles at 95°C for 30 s, 55°C for 30 s, and 72°C for 1 min; and a final extension at 72°C for 7 min. The specific primers used for PCRs are as follows: HEK293T cells, $Ca_V2.1$ forward (5′-TGGAATCAGCGTGTTACGAG-3′) and reverse (5′-GCGGACAGAGGACTCACTTC-3′); cortical neurons, $Ca_V2.1$ forward (5′-TGGAATCAGCGTGTTACGAG-3′), and reverse (5′-GCAGACAGGGGACTCACTTC-3′); and GAPDH forward (5′-CAAGGTCATCCATGACAACTTTG-3′), and reverse (5′-GTCCACCACCCTGTTGCTGTAG-3′). The predicted sizes of the amplified PCR fragment for $Ca_V2.1$ and GAPPDH are ~500 and 496 bp, respectively. RT-PCR products were resolved by electrophoresis in 1.7% agarose gels, followed by quantification with ImageJ.

Cycloheximide chase. At 24 h after transfection, cells were subjected to treatment with the protein synthesis inhibitor cycloheximide (100 μg/ml; Sigma-Aldrich) for 0–6 h, followed by immunoblotting. Quantitative analyses of protein degradation time course under various coexpression conditions were implemented by standardizing $Ca_V2.1$ protein densities in response to different CHX treatment durations as the ratio of $Ca_V2.1$ signal to the cognate tubulin signal, followed by normalization to the corresponding vector control at 0 h. The logarithmic value of normalized attenuation of $Ca_V2.1$ protein density was in turn plotted against a linear scale of CHX treatment duration (the semilogarithmic plot). The $Ca_V2.1$ protein half-life value was then derived from single/double linear-regression analysis of the semilogarithmic plot. For a given experimental condition with multiple repeats, an individual $Ca_V2.1$ protein half-life value was determined from each single trial, followed by data pooling and statistical analyses.

Protein ubiquitination analyses. Cells were solubilized in lysis buffer supplemented with 2.5 mg/ml *N*-ethylmaleimide, followed by immunoprecipitation with the anti-Myc antibody as described above. To facilitate the visualization of ubiquitination signals associated with proteins of high molecular weight, a 7% SDS-PAGE protocol involving a gel running time over 2 h was used.

Biotinylation of cell surface proteins. Transfected cells were washed extensively with D-PBS (Sigma-Aldrich) supplemented with 0.5 mM $CaCl_2$, 2 mM $MgCl_2$, followed by incubation in 1 mg/ml sulfo-NHS-LC-biotin (Thermo Scientific) in D-PBS at 4°C for 1 h with gentle rocking. Biotinylation was terminated by removing the biotin reagents and rinsing three times with 100 mM glycine in PBS, followed by once in TBS buffer containing the following (in mM): 20 Tris-HCl and 150 NaCl, pH 7.4. Cells were solubilized in a lysis buffer containing the following (in mM): 150 NaCl, 50 Tris-HCl, 1% Triton X-100, 5 EDTA, 1 PMSF, pH 7.6 supplemented with the protease inhibitor mixture. Insolubilized materials were removed by centrifugation. Solubilized cell lysates were incubated over-

night at 4°C with streptavidin-agarose beads (Thermo Scientific). Beads were washed once in the lysis buffer, followed by twice in a high-salt buffer containing the following (in mM): 500 NaCl, 5 EDTA, 50 Tris-HCl, pH 7.6, 0.1% Triton X-100 and once in a low-salt buffer containing the following (in mM): 2 EDTA, 10 Tris-HCl, pH 7.6, 0.1% Triton X-100. The biotin–streptavidin complexes were eluted from the beads by heating at 70°C for 5 min in the Laemmli sample buffer.

Electrophysiological recordings. Both Xenopus oocytes and HEK293T cells were used for functional studies of human $Ca_V2.1$ currents. For *in vitro* transcription, cDNAs were linearized with appropriated restriction enzymes as described previously (Jeng et al., 2006). Capped cRNAs were transcribed from the linearized cDNA template with the mMessage mMachine T7 kit (Ambion). For cRNA injection, adult female *Xenopus laevis* (African *Xenopus* Facility) were anesthetized by immersion in ice water containing Tricaine (1.5 g/L). Ovarian follicles were removed from *Xenopus* frogs, cut into small pieces, and incubated in the ND96 solution containing the following (in mM): 96 NaCl, 2 KCl, 1.8 $MgCl_2$, 1.8 $CaCl_2$, and 5 HEPES, pH 7.2. To remove the follicular membrane, *Xenopus* oocytes were incubated in the Ca^{2+}-free ND96 solution containing collagenase (2 mg/ml) on an orbital shaker (~200 rpm) for ~60–90 min at room temperature. After several washes with collagenase-free, Ca^{2+}-free ND96, oocytes were transferred to ND96. Stage V–VI *Xenopus* oocytes were then selected for cRNA injection. Unless stated otherwise, cRNAs (and cDNAs) for α_{1A}, $\alpha_2\delta$, and β_4 were mixed in a molar ratio of 1:2:2 and the final injection amounts (total volume: 41.4 nl) for α_{1A}, α_2, and β_4 cRNAs were ~3.8 ng, ~3.8 ng, and ~1.9 ng per oocyte, respectively. Injected oocytes were stored at 16°C in ND96. 2–3 d after cRNA injection, *Xenopus* oocytes were transferred into a recording bath (~200 μl) containing the following (in mM): 40 $Ba(OH)_2$, 50 NaOH, 2 CsOH, 5 HEPES, and 0.4 niflumic acid, pH 7.4 with methanesulfonic acid. An agarose bridge was used to connect the bath solution to a ground chamber (containing 3 M KCl), into which two ground electrodes were inserted. Borosilicate electrodes (0.1–1 MΩ) used in voltage recording and current injection were filled with 3 M KCl. Ba^{2+} currents through $Ca_V2.1$ channels were acquired using the conventional two-electrode voltage-clamp technique with an OC-725C oocyte clamp (Warner Instruments).

Conventional whole-cell patch-clamp technique was performed in HEK293T cells. Transfected cells were identified by GFP fluorescence (the cDNAs for $Ca_V2.1$ and pEGFP were cotransfected in the molar ratio 1:0.05) with an inverted fluorescence microscope (Leica DM IRB). Recording electrodes (2–4 MΩ) were pulled by a PP-830 puller (Narashige). The pipette solution contained the following (in mM): 145 CsCl, 3 $MgCl_2$, 5 EGTA, 10 HEPES, 2 Mg-ATP, and 0.4 Na-GTP, pH 7.3. The bath solution contained the following (in mM): 10 $BaCl_2$, 135 TEA · Cl, 4 KCl, 1 $MgCl_2$, and 10 HEPES, pH 7.2. Data were acquired and digitized with Axopatch 200B and Digidata 1440A, respectively, via pCLAMP 10.2 (Molecular Devices, RRID: SCR_011323). Cell capacitances were measured using the built-in functions of pCLAMP 10.2 and were compensated electronically with Axopatch 200B. The holding potential was set at −90 mV and passive membrane properties were compensated using the −P/4 leak subtraction method provided by the pCLAMP software. Data were sampled at 10 kHz and filtered at 1 kHz. All recordings were performed at room temperature (20–22°C).

To avoid the potential biases imposed by variations in $Ca_V2.1$ WT channel expression among different oocytes, we adopted a previously reported data normalization procedure (Jeng et al., 2006). Briefly, for the same batch of oocytes on a given day of experimentation, the average value of the peak Ba^{2+} current amplitudes of $Ca_V2.1$ WT channels under each coexpression condition was normalized to that of $Ca_V2.1$ WT vector control. Normalized data from different batches of *Xenopus* oocytes on different dates were later pooled together for comprehensive analysis. A similar Ba^{2+} current density normalization and data pooling strategy was also applied to the HEK293T cell system

Statistical analyses. All values are presented as mean ± SEM. The significance of the difference between two means was tested using Student's *t* test, whereas means from multiple groups were compared using one-way ANOVA analysis. All statistical analyses were performed with Origin version 7.0 (Microcal Software, RRID:SCR_002815).

Results

Interaction and colocalization of RNF138 with $Ca_V2.1$ in neurons

In the human brain, a short and a long $Ca_V2.1$ subunit splice variant, with a difference in the size of the cytoplasmic C-terminal region by ~234 aa, are generated by the differential use of the splice acceptor at the boundary of intron 46 and exon 47 of the *CACNA1A* gene: the short $Ca_V2.1$ isoform contains a stop codon immediately after exon 46, whereas the long isoform contains a much longer C-terminal tail encoded by exon 47 (Soong et al., 2002; Adams et al., 2009; Lipscombe et al., 2013). In the mammalian expression system, EA2 mutant-induced dominant-negative effects were reported previously for both the short and the long $Ca_V2.1$ isoforms (Jeng et al., 2008; Mezghrani et al., 2008). Because approximately two-thirds of the transcripts of the *CACNA1A* gene in the human cerebellum are composed of the long isoform (Soong et al., 2002), herein we focus on the long $Ca_V2.1$ isoform.

We performed yeast two-hybrid screening of a rat brain cDNA library with a bait vector encoding the distal C-terminal region ($Ca_V2.1$-C-ter) of the long isoform of human $Ca_V2.1$ subunit (see Materials and Methods for more details) and obtained a total of 67 independent prey clones, including two previously reported $Ca_V2.1$-interacting proteins: endophilin and RIM-binding protein (Chen et al., 2003; Kaeser et al., 2011). Importantly, we identified RNF138 as a potential binding partner of $Ca_V2.1$. RNF138, also known as NARF, contains a RING finger domain near its N terminus (Anderson et al., 2010) and was demonstrated to be an E3 ubiquitin ligase negatively regulating the Wnt-β-catenin signaling pathway in *Xenopus* embryos (Yamada et al., 2006). In neurons, RNF138 may serve as a binding partner of the small integrin-binding ligand osteopontin (Long et al., 2012). Moreover, RNF138 appears to contribute to tumorigenesis of gliomas and regulation of cell death (Anderson et al., 2010; Zhou et al., 2012; Brooks et al., 2014). Overall, little is known about the molecular nature of RNF138 substrate proteins in the brain.

We verified the interaction between RNF138 and $Ca_V2.1$ with a GST pull-down assay using a GST fusion protein comprising the $Ca_V2.1$-C-ter fragment (Fig. 1*B*, left). Moreover, systemic pull-down assays with GST fusion proteins comprising additional intracellular domains of $Ca_V2.1$ indicate that the N-terminal region and the linker connecting transmembrane domains II and III of $Ca_V2.1$ also contribute to the RNF138 interaction (Fig. 1*B*, right). The interaction between RNF138 and $Ca_V2.1$ was further confirmed by immunoprecipitation experiment with the full-length human $Ca_V2.1$ subunit (Fig. 1*C*) in the HEK293T heterologous expression system.

Figure 2*A* shows that, in rat forebrain lysates, endogenous RNF138 was coimmunoprecipitated with $Ca_V2.1$, consistent with the idea that the two molecules coexist in the same protein complex in native neurons. We also examined the subcellular localization of these proteins in neurons by performing sucrose gradient centrifugation analyses of rat forebrain homogenates. In the synaptic region, $Ca_V2.1$ channels are localized at both presynaptic axon terminals and postsynaptic dendritic spines (Westenbroek et al., 1995; Sakurai et al., 1996; Koester and Sakmann, 2000; Lee et al., 2002; Kulik et al., 2004). As depicted in Figure 2*B*, both RNF138 and $Ca_V2.1$ are highly enriched in the SPM fraction, as well as in the SPM subfractions PSD I and PSD II, implying a colocalization of the two proteins at presynaptic and postsynaptic compartments. Moreover, we studied the subcellular localization of RNF138 and $Ca_V2.1$ in cultured cortical neurons prepared from rat embryos. Figure 2*C* demonstrates that,

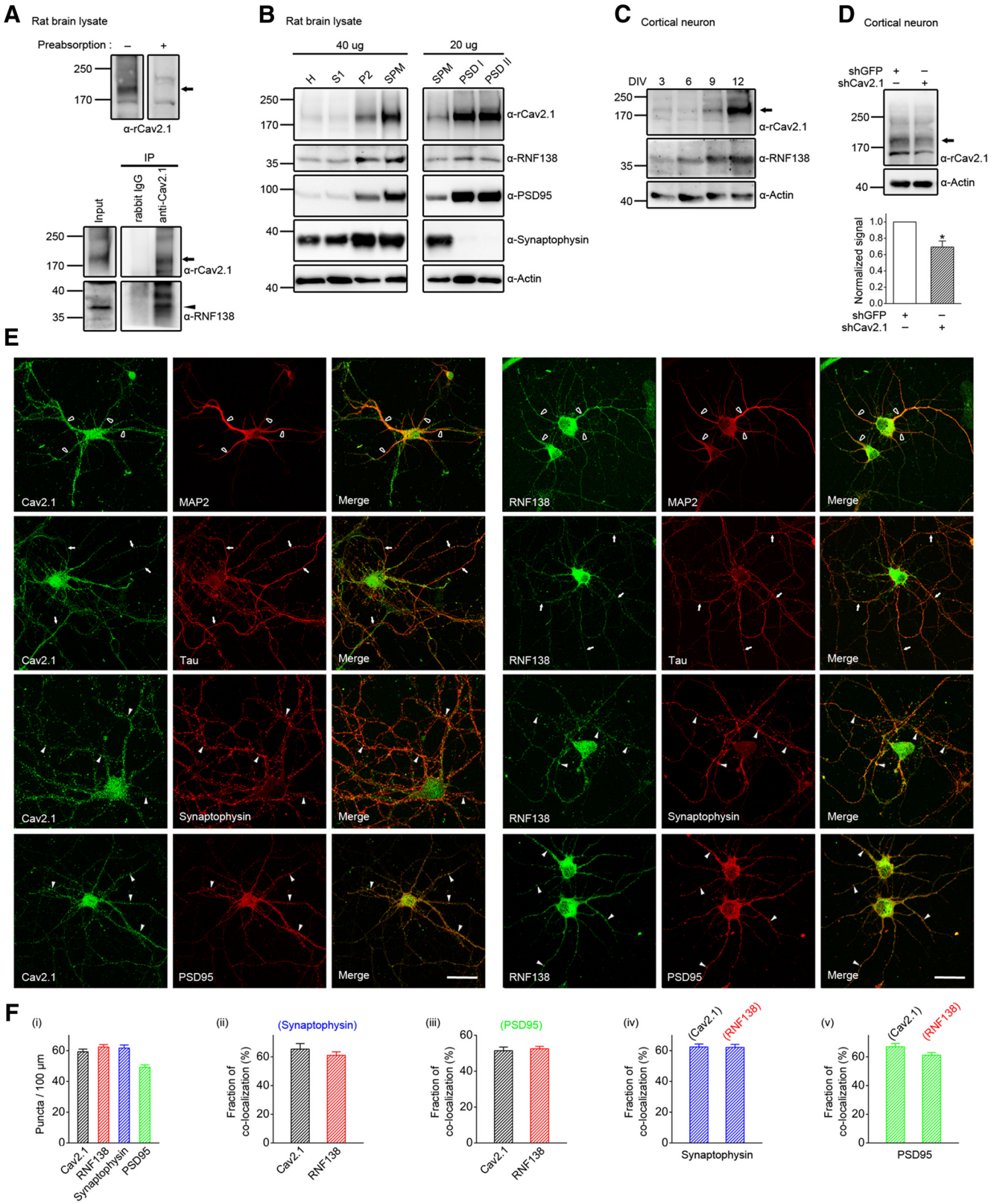

Figure 2. Colocalization of RNF138 and $Ca_V2.1$ in neurons. ***A***, Interaction of rat $Ca_V2.1$ and RNF138 in the brain. Top, Verification of the specificity of the anti-rat $Ca_V2.1$ antibody (α-r$Ca_V2.1$). Rat $Ca_V2.1$ protein detection was prevented by preabsorbing the immunoblot with a control antigen peptide. Endogenous $Ca_V2.1$ in the rat brain comprises a major isoform with an apparent molecular weight of ~190 kDa (labeled with black arrows), as well as a minor isoform of ~220 kDa (Sakurai et al., 1995; Westenbroek et al., 1995). Bottom, Coimmunoprecipitation of endogenous RNF138 with $Ca_V2.1$. Rat forebrain lysates were immunoprecipitated with α-r$Ca_V2.1$ or the rabbit IgG. The protein band corresponding to rat RNF138 is highlighted with black arrowhead. ***B***, Colocalization of rat $Ca_V2.1$ and RNF138 at presynaptic and postsynaptic compartments. Subcellular fractionation separated rat brains into homogenate (H), soluble (S1), crude membrane (P2), synaptosomal (SPM), and two postsynaptic density (PSD I, PSD II) fractions. Synaptophysin and PSD-95 serve as the presynaptic and the postsynaptic markers, respectively. The terms 40 μg and 20 μg refer to the amount of total protein loaded in each lane. ***C***, Developmental protein expression patterns of rat $Ca_V2.1$ and RNF138 in cultured cortical neurons with different (*Figure legend continues.*)

comparing neurons at different days in culture, the protein expression level of RNF138 gradually increased from DIV3 and appeared to stabilize by DIV12. In contrast, $Ca_V2.1$ expression was not observed until DIV9. We therefore chose DIV10 neurons for further morphological analyses. In addition to the antigen peptide preabsorption experiment in brain lysates (Fig. 2*A*), the specificity of the anti-rat $Ca_V2.1$ antibody was further verified in cultured neurons subjected to shRNA suppression of endogenous $Ca_V2.1$ level (Fig. 2*D*). In brain sections, $Ca_V2.1$ subunits are characterized by a distinct punctate immunostaining pattern that reflects their abundant localization at synapses (Westenbroek et al., 1995; Sakurai et al., 1996; Lee et al., 2002). Figure 2*E* exemplifies the immunofluorescence signals of endogenous $Ca_V2.1$ and RNF138 in cultured cortical neurons. Consistent with previous findings in brain sections, $Ca_V2.1$ subunits in both dendrites (MAP2-positive neurites) and axons (tau-positive neurites) of cultured cortical neurons display notable punctate patterns that appear to colocalize with the presynaptic and postsynaptic markers synaptophysin and PSD-95, respectively (Fig. 2*E*, left). Compared with $Ca_V2.1$, RNF138 displays a diffuse immunofluorescence pattern in both axonal and dendrosomatic regions (Fig. 2*E*, right). Nevertheless, like $Ca_V2.1$, RNF138 also shows prominent patterns of punctate staining at presynaptic and postsynaptic sites. Furthermore, $Ca_V2.1$ and RNF138 display quantitatively comparable colocalization with the synaptic proteins synaptophysin and PSD-95 (Fig. 2*F*). Collectively, the preceding observations strongly support the physical association and colocalization of endogenous RNF138 with $Ca_V2.1$ in neurons.

RNF138 is an E3 ubiquitin ligase of $Ca_V2.1$

To characterize the functional significance of the RNF138–Cav2.1 interaction, we first examined the effect of rat RNF138 overexpression on human Cav2.1 total protein level in HEK293T cells. Figure 3*A* illustrates that Cav2.1 protein expression decreases by ~60% in the presence of RNF138; in contrast, no detectable effect was observed when we coexpressed Cav2.1 with another RING finger E3 ubiquitin ligase, RNF128 (Lineberry et al., 2008). Figure 3*B* further demonstrates that, despite the lack of >200 aa in the C-terminal region, the short isoform of Cav2.1 subunit also exhibits a significant reduction in total protein level by ~58% in response to RNF138 overexpression. In contrast, RNF138 displays no discernible effect on Cav1.2 (L-type) or $Ca_V2.2$ (N-type) subunits. The suppression of RNF138 on Cav2.1 protein level is effectively reversed by treatment with the proteasome inhibitor MG132 (Fig. 3*C*), suggesting that the observed Cav2.1 suppression effect may involve RNF138-mediated proteasomal degradation.

RNF138 contains a C_3HC_4-type RING (RING-HC) finger domain that is present in many E3 ubiquitin ligases (Deshaies and Joazeiro, 2009; Anderson et al., 2010). Moreover, a highly conserved histidine residue (H36 in both rat and human RNF138) in this RING finger domain plays an essential role in coordinating zinc binding, which is required for maintaining the overall structure of the RING domain. Mutation of this highly conserved histidine residue (e.g., being replaced by a glutamate residue) disrupts the enzyme activity of RING finger E3 ubiquitin ligase (Kim et al., 2005). We therefore created a point mutation construct (RNF138-H36E) to investigate how this mutant may affect protein expression of $Ca_V2.1$. Figure 3*D* shows that overexpression of rat RNF138-H36E dramatically increases $Ca_V2.1$ protein level by ~72% in HEK293T cells. Rat and human RNF138 share ~92% identity in their amino acid sequences. We also demonstrated that $Ca_V2.1$ protein expression in HEK293T cells is reduced by human RNF138 (hRNF138), but is enhanced by an N-terminal deletion mutant lacking the critical RING finger domain (hRNF138-ΔN; Fig. 3*E*). Together, these observations are consistent with the idea that both the rat and the human RNF138 mutants may prevent $Ca_V2.1$ protein degradation by endogenous RNF138 in HEK293T cells. Consistent with this notion, shRNA knock-down of endogenous RNF138 expression in HEK293T cells substantially increases $Ca_V2.1$ protein level by ~43% (Fig. 3*F*). To rule out the possibility that the foregoing results may simply be an artifact associated with the non-neuron HEK293T expression system, we repeated the shRNA knock-out experiment using human neuroblastoma NT2 cells and obtained virtually identical $Ca_V2.1$ enhancement results (Fig. 3*F*). Furthermore, by suppressing endogenous rat RNF138 expression in cultured cortical neurons, we also observed a robust upregulation of endogenous rat $Ca_V2.1$ protein expression by ~46–89% (Fig. 3*G*).

The RNF138-induced $Ca_V2.1$ protein suppression effect may in theory arise from either reduced protein synthesis or enhanced protein degradation. Coexpression with RNF138 or RNF138-H36E fails to measurably alter $Ca_V2.1$ mRNA level in HEK293T cells (Fig. 4*A*). In addition, shRNA knock-down of endogenous rat RNF138 does not discernibly affect $Ca_V2.1$ mRNA level in cultured cortical neurons (Fig. 4*B*). Conversely, by performing cycloheximide chase experiments, we found that, in the presence of RNF138, $Ca_V2.1$ protein half-life was reduced dramatically from ~8.1 h to ~3.1 h (single linear-regression fit; or to ~1.3 and 5.5 h; double linear-regression fit; Fig. 4*C*,*D*). In contrast, overexpressing the RNF138-H36E mutant significantly increases $Ca_V2.1$ protein half-life to ~10.9 h (Fig. 4*C*,*D*). In comparison, RNF128 overexpression exerts no detectable effect on the protein turnover rate of $Ca_V2.1$ subunit (protein half-life: ~8.7 h; Fig. 4*C*,*D*). Moreover, shRNA knock-down of endogenous RNF138 in HEK293T cells prolongs $Ca_V2.1$ protein half-life to ~10.3 h (Fig. 4*E*,*F*). Overall, these results confirm that RNF138 downregulates $Ca_V2.1$ protein level through enhanced protein degradation.

To further test the hypothesis that RNF138 serves as an E3 ubiquitin ligase of $Ca_V2.1$, we then investigated whether RNF138

←

(*Figure legend continued.*) DIV. ***D***, Suppression of endogenous $Ca_V2.1$ level in cultured cortical neurons infected with shRNA for $Ca_V2.1$ ($shCa_V2.1$). shRNA for GFP (shGFP) was used as the infection control. For quantitative analyses of relative $Ca_V2.1$ protein level, $Ca_V2.1$ signals were standardized as the ratio to the β-actin loading control, which were then normalized to the shGFP infection control ($n = 4$). Asterisk denotes significant difference from the infection control (*$p < 0.05$). ***E***, Representative confocal microscopic images of rat $Ca_V2.1$ (left) and RNF138 (right) immunofluorescence signals in DIV10 cortical neurons. First row, Distribution of $Ca_V2.1$ or RNF138 (green) along MAP2-positive (red) dendrites and somas, which is highlighted with white triangles and further demonstrated in the merge images. Second row, Distribution of $Ca_V2.1$ or RNF138 (green) along tau-positive (red) axons, which is highlighted with white arrows. Third and fourth rows, White arrowheads highlight the colocalization of $Ca_V2.1$ or RNF138 puncta (green) with synaptophysin or PSD95 puncta (red) along neurites, which is further indicated as yellow puncta in the merge images. Scale bar, 50 μm. ***F***, Quantification of puncta density (puncta/100 μm) and puncta colocalization ratio (fraction of colocalization) in DIV10 cortical neurons. The analyses were based on 15–30 individual neurites associated with 3–6 different neurons. ***Fi***, Estimated puncta densities per 100 μm neurite are ~59.3 ± 1.8 ($Ca_V2.1$), 62.4 ± 1.6 (RNF138), 61.7 ± 2.0 (synaptophysin), and 49.2 ± 1.6 (PSD95). ***Fii***, The estimated synaptophysin colocalization ratios are ~65.4 ± 3.9% ($Ca_V2.1$) and 61.1 ± 2.4% (RNF138). ***Fiii***, Estimated PSD95 colocalization ratios are ~51.4 ± 2.1% ($Ca_V2.1$) and 52.5 ± 1.4% (RNF138). ***Fiv–Fv***, Conversely, for synaptophysin, the estimated $Ca_V2.1$ and RNF138 colocalization ratios are ~62.4 ± 2.0% and 62.2 ± 2.0%, respectively; for PSD95, the estimated $Ca_V2.1$ and RNF138 colocalization ratios are ~67.0 ± 2.3% and 61.2 ± 1.8%, respectively.

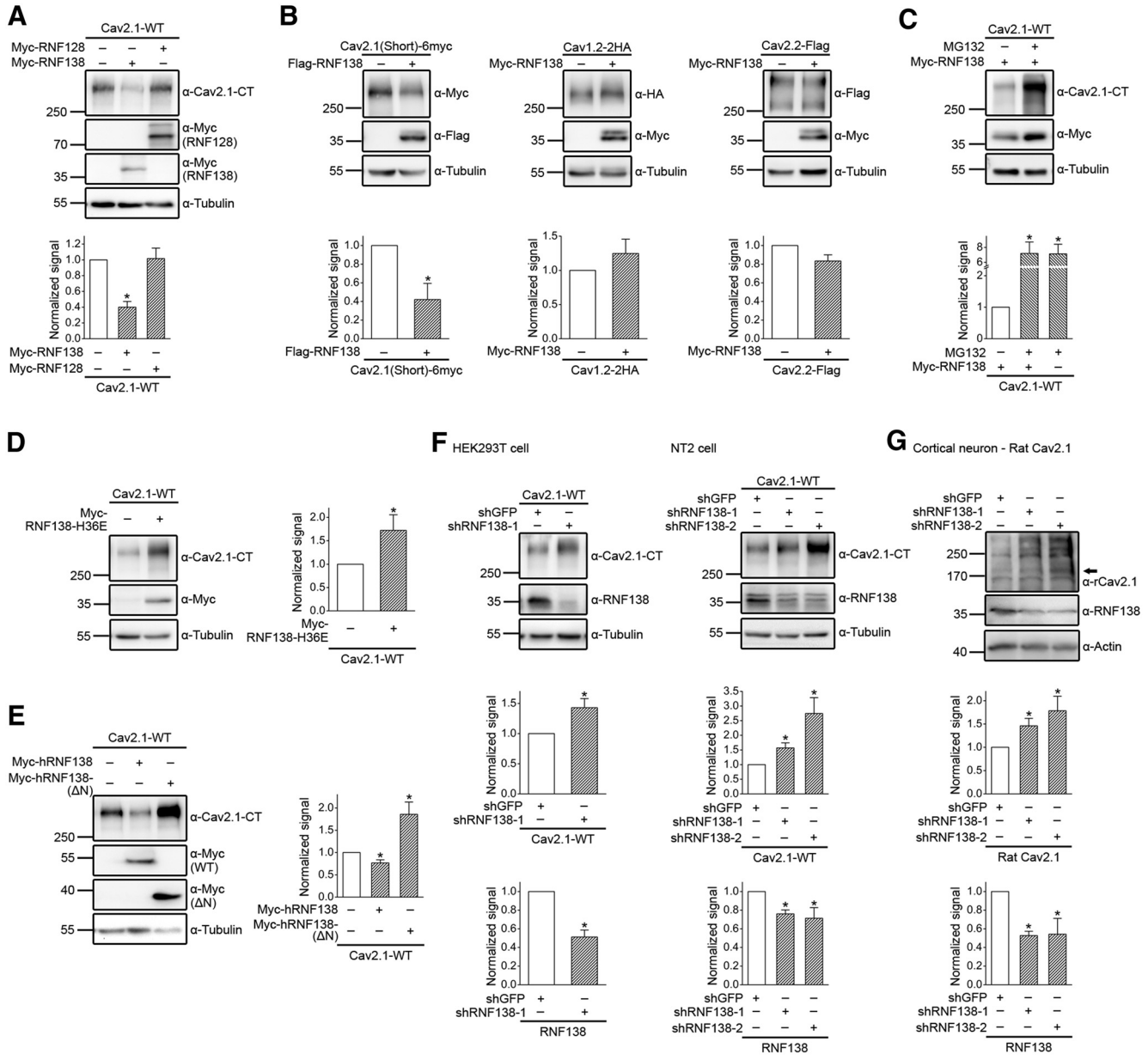

Figure 3. Regulation of $Ca_V2.1$ protein expression by RNF138. ***A***, Human $Ca_V2.1$ long-isoform ($Ca_V2.1$-WT) was coexpressed with the Myc vector (−), Myc-tagged rat RNF138 (Myc-RNF138), or Myc-tagged human RNF128 (Myc-RNF128) in the molar ratio of 1:3 in HEK293T cells. Top, Representative $Ca_V2.1$ protein level in response to different coexpression conditions. Bottom, Quantification of relative $Ca_V2.1$ protein level. $Ca_V2.1$ signals were standardized as the ratio to the cognate loading control, followed by normalization to the corresponding vector control ($n = 6–12$). ***B***, Coexpression of rat RNF138 (Flag-RNF138 or Myc-RNF138) with Myc-tagged human $Ca_V2.1$ short-isoform [$Ca_V2.1$(Short)-6myc; ~260–270 kDa], HA-tagged rat $Ca_V1.2$ ($Ca_V1.2$-HA; ~260 kDa), or Flag-tagged bovine $Ca_V2.2$ ($Ca_V2.2$-Flag; ~255–280 kDa) in HEK293T cells. For quantification, data in each coexpression condition were normalized to the vector control ($n = 3–4$). ***C***, Treatment with 10 μM MG132 for 24 h reverses RNF138-mediated suppression of $Ca_V2.1$ protein level in HEK293T cells. Data were normalized to the DMSO treatment (−) control ($n = 6–9$). ***D***, Effect of Myc-tagged rat RNF138-H36E (Myc-RNF138-H36E) on $Ca_V2.1$ protein level in HEK293T cells ($n = 12$). ***E***, Effect of Myc-tagged human RNF138 (Myc-hRNF138) wild-type (WT) and N-terminal (residues 1–64) deletion mutant (Myc-hRNF138-ΔN) on $Ca_V2.1$ protein level in HEK293T cells ($n = 5$). ***F***, Suppression of endogenous RNF138 expression with shRNA for RNF138 (shRNF138-1, shRNF138-2) enhances $Ca_V2.1$ protein level in HEK293T (left) and human neuroblastoma NT2 (right) cells. Data were normalized to the shRNA for GFP (shGFP) infection control ($n = 5–6$). ***G***, shRNA-mediated silencing of endogenous rat RNF138 expression results in the upregulation of endogenous rat $Ca_V2.1$ protein level in cultured cortical neurons ($n = 5$). The arrow refers to the major, 190 kDa rat $Ca_V2.1$ isoform. Tubulin or actin signals were used as loading control and for quantification standardization. Asterisks denote significant difference from the control ($^*p < 0.05$).

regulates protein ubiquitination of $Ca_V2.1$ subunit. We began by addressing how ubiquitin molecules are attached to $Ca_V2.1$. Ubiquitination in general involves covalent linkage of lysine residues with single/multiple monoubiquitins or with polyubiquitin chains that are also formed by covalent linkage of lysine (Abriel and Staub, 2005; Kravtsova-Ivantsiv and Ciechanover, 2012). Therefore, polyubiquitination, but not monoubiquitination, becomes virtually impossible if all of the lysine residues within ubiquitin are replaced by arginine (known as the lysine-less ubiquitin mutant, Ub-K0). For a given protein, if polyubiquitin chain formation is required for its degradation, then overexpressing the Ub-K0 mutant may effectively enhance its steady-state protein expression (Bloom et al., 2003; Volk et al., 2005). Figure 5*A* shows that Ub-K0 overexpression prominently upregulates $Ca_V2.1$ protein level by ~74%; in contrast, coexpression with ubiquitin WT (Ub-WT) significantly reduces $Ca_V2.1$ protein level by ~23%. These

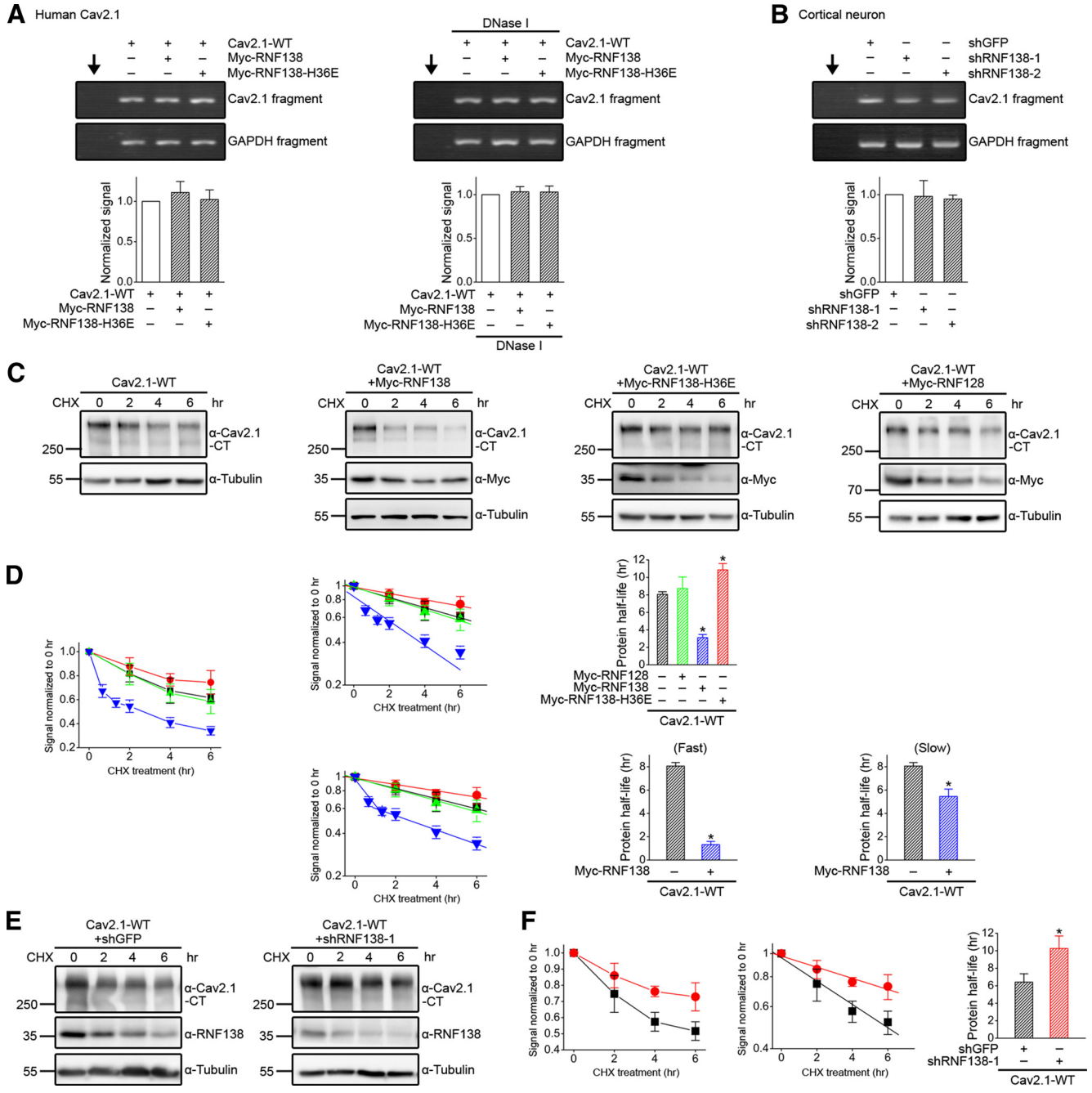

Figure 4. RNF138 reduces $Ca_V2.1$ protein stability. ***A***, Lack of effect of RNF138/RNF138-H36E overexpression on human $Ca_V2.1$ mRNA level in HEK293T cells subject to the indicated transfection condition ($p > 0.05$; $n = 3$). To rule out the potential contamination arising from human $Ca_V2.1$ plasmid in RNA prepared from transfected cells, RT-PCR was performed in the absence (left) or presence (right) of DNase I treatment before reverse transcription reaction. Also shown is the blank control that involves identical PCR in the absence of cDNA template (vertical arrows). The signals of $Ca_V2.1$ were standardized as the ratio to those of cognate GAPDH, followed by normalization to the corresponding Myc vector control. ***B***, RNF138 knock-down does not significantly change rat $Ca_V2.1$ mRNA level in neurons ($p > 0.05$; $n = 3$). RT-PCR analyses were based on RNA extracted from cultured cortical neurons subject to the indicated shRNA infection. Standardized $Ca_V2.1$ signals were normalized to the shGFP infection control. ***C***, Representative immunoblots showing the effect of RNF128, RNF138, or RNF138-H36E coexpression on protein stability of human $Ca_V2.1$ subunit. $Ca_V2.1$ protein turnover kinetics in HEK293T cells was analyzed by applying cycloheximide (CHX) with the indicated treatment durations (h). Coexpression with the Myc vector was used as the control experiment. ***D***, Quantification of $Ca_V2.1$ protein half-life in the presence of Myc vector (black), RNF128 (green), RNF138 (blue), or RNF138-H36E (red). Left, Normalized $Ca_V2.1$ protein densities with respect to cycloheximide treatment durations. Data points represent the average of 7–8 independent experiments. Center, Same data points were transformed into a semilogarithmic plot, which is subject to single linear-regression analyses (solid lines; top) or double linear-regression analyses (solid lines; bottom with RNF138 only). Right, Comparison of $Ca_V2.1$ protein half-life values derived from linear-regression analyses. The estimated $Ca_V2.1$ protein half-life values based on single linear-regression analyses (top right) are ~8.1 ± 0.3 (with vector; $n = 8$), 8.7 ± 1.3 (with RNF128; $n = 7$), 3.1 ± 0.4 (with RNF138; $n = 8$), and 10.9 ± 0.7 (with RNF138-H36E; $n = 8$) h. Based on double linear-regression analyses (bottom right), the estimated $Ca_V2.1$ protein half-life values in the presence of RNF138 are ~1.3 ± 0.3 h (fast component) and 5.5 ± 0.6 h (slow component). ***E***, Representative immunoblots showing the effect of shRNA knock-down of endogenous RNF138 on $Ca_V2.1$ protein turnover kinetics in HEK293T cells. shGFP infection was used as the control experiment. ***F***, Quantification and comparison of $Ca_V2.1$ protein half-life values derived from different shRNA infection conditions. The estimated $Ca_V2.1$ protein half-life values are ~6.4 ± 1.0 h (with shGFP; $n = 9$; black) and 10.3 ± 1.4 h (with shRNF138 –1; $n = 9$; red). The protein half-life value of $Ca_V2.1$ in the presence of shGFP is not statistically different ($p > 0.05$) from that of $Ca_V2.1$ with vector in ***D***. Asterisks denote significant difference from the control (*$p < 0.05$).

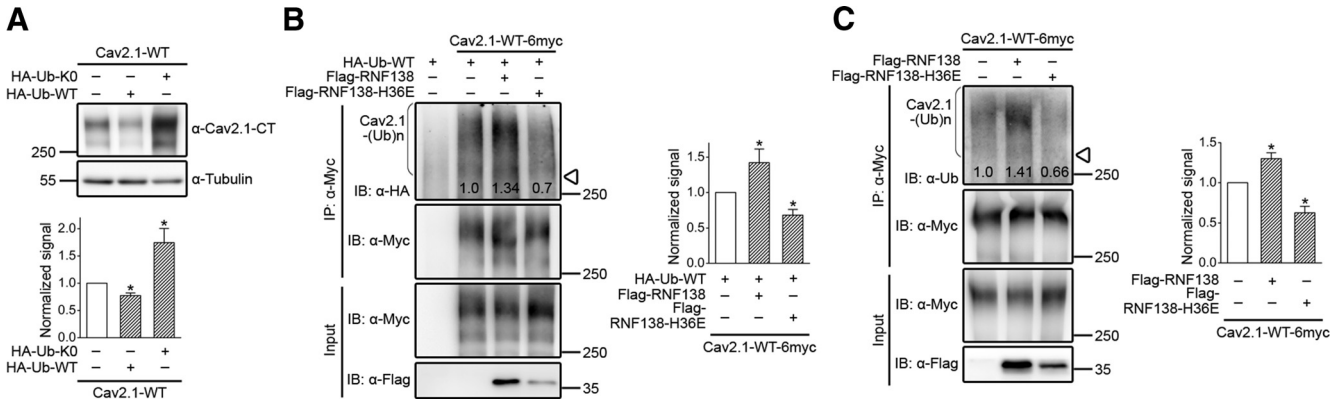

Figure 5. RNF138 promotes $Ca_V2.1$ polyubiquitination. Biochemical demonstration of $Ca_V2.1$ polyubiquitination in HEK293T cells. ***A***, Top, Representative immunoblots showing the effect of HA-tagged human lysine-less ubiquitin mutant (HA-Ub-K0) or ubiquitin wild-type (HA-Ub-WT) coexpression on $Ca_V2.1$ protein level. Coexpression with the HA vector was used as the control experiment. The relative molar ratio to $Ca_V2.1$ was 1:1. Bottom, Quantification of relative $Ca_V2.1$ protein level. Standardized $Ca_V2.1$ signals were normalized to the HA vector control ($n = 6–9$). ***B***, Effect of coexpressing Flag-RNF138 or Flag-RNF138-H36E on Myc-tagged $Ca_V2.1$ WT ($Ca_V2.1$-WT-6myc) polyubiquitination [$Ca_V2.1$-(Ub)n] by HA-Ub-WT. Left, Cell lysates were immunoprecipitated with α-Myc, and protein ubiquitination was recognized by immunoblotting with the anti-HA antibody (α-HA). The no-$Ca_V2.1$ lane exemplifies the background HA-Ub-WT signal in the absence of $Ca_V2.1$. Corresponding expression levels of $Ca_V2.1$ and RNF138 in the lysates are shown in the "input" lane. Ubiquitinated $Ca_V2.1$ is visualized as high-molecular-weight protein smears. Open triangles refer to the expected location of the protein band corresponding to nonubiquitinated $Ca_V2.1$. The numbers shown on the immunoblots denote densitometric quantification of relative $Ca_V2.1$ ubiquitination with respect to the HA-Ub-WT control. Right, Normalized $Ca_V2.1$ ubiquitination signals from multiple experiments were compiled for statistical analyses ($n = 4–6$), with the mean relative values 1.4 ± 0.2 (with RNF138) and 0.7 ± 0.1 (with RNF138-H36E). ***C***, Effect of Flag-RNF138 and Flag-RNF1388-H36E on $Ca_V2.1$ polyubiquitination by endogenous ubiquitin in HEK293T cells. Protein ubiquitination was identified by immunoblotting with the anti-ubiquitin antibody (α-Ub). $Ca_V2.1$ ubiquitination signals were normalized to the Flag vector control ($n = 7–8$), with the mean relative values 1.3 ± 0.1 (with RNF138) and 0.6 ± 0.1 (with RNF138-H36E). Asterisks denote significant difference from the control ($^*p < 0.05$).

results imply that, before its degradation, the $Ca_V2.1$ subunit is subject to substantial polyubiquitination. Figure 5, *B* and *C*, further illustrate that, by immunoblotting with specific antibodies against either overexpressed HA-tagged ubiquitin or endogenous ubiquitin in HEK293T cells, $Ca_V2.1$ polyubiquitination was detected directly as a smear of high-molecular-weight protein bands. Importantly, the extent of $Ca_V2.1$ polyubiquitination was enhanced and attenuated by RNF138 and the H36E mutant, respectively.

So far, we have only described the effect of RNF138 on $Ca_V2.1$ subunit per se. Nevertheless, a functional $Ca_V2.1$ channel comprises a $Ca_V2.1$ subunit, as well as the auxiliary $\alpha_2\delta$ and β subunits. Emerging evidence strongly suggests that β subunits may protect nascent $\alpha1$ (e.g., $Ca_V1.2$ and $Ca_V2.2$) subunits in the ER from polyubiquitination and that the $\alpha_2\delta$ subunits may facilitate forward trafficking of nascent $\alpha1$ (e.g., $Ca_V1.2$, $Ca_V2.1$, and $Ca_V2.2$) subunits out of the ER (Cantí et al., 2005; Altier et al., 2011; Waithe et al., 2011; Page et al., 2016). In agreement with these observations, Figure 6*A* depicts that coexpression with β_{1b}, $\beta2a$, or β_{4a} subunits indeed significantly attenuate Myc-RNF138-mediated $Ca_V2.1$ protein degradation. Likewise, Myc-RNF138-mediated $Ca_V2.1$ protein degradation is also notably reduced in the presence of $\alpha_2\delta$ subunit (Fig. 6*B*). Moreover, coexpression with $\alpha_2\delta$ and β_{4a} subunits effectively diminishes the effect of Flag-RNF138 on $Ca_V2.1$ protein turnover and polyubiquitination (Fig. 6*C*,*D*). We also investigated the effect of $\alpha_2\delta$ and β_{4a} subunits on $Ca_V2.1$ in the absence of Myc/Flag-RNF138 overexpression. Overexpressing $\alpha_2\delta$ and β_{4a} subunits leads to significant upregulation of $Ca_V2.1$ level (Fig. 6*E*), deceleration of $Ca_V2.1$ turnover kinetics (Fig. 6*F*), and reduction of $Ca_V2.1$ polyubiquitination (Fig. 6*G*), consistent with the idea that the auxiliary subunits notably attenuate $Ca_V2.1$ degradation by endogenous RNF138 in HEK293T cells. Interestingly, these results further suggest that the RNF138–ubiquitin–proteasome system may effectively prevent ER exiting of $Ca_V2.1$ subunits not coassembled with auxiliary $\alpha_2\delta$ and β subunits.

RNF138 mediates proteasomal degradation of EA2-causing $Ca_V2.1$ mutants

Previous experimental evidence clearly demonstrates that the EA2-causing human $Ca_V2.1$ nonsense (truncation) mutant R1281X and the missense mutant F1406C display prominent loss-of-function phenotypes (Jen et al., 2001; Wappl et al., 2002; Jeng et al., 2006). The $Ca_V2.1$ R1281X mutation is caused by a premature stop codon in the extracellular loop linking transmembrane S1–S2 segments of domain III, whereas $Ca_V2.1$ F1406C involves a point mutation at the pore-loop region of domain III. In addition, R1281X is subject to significant proteasomal degradation (Mezghrani et al., 2008). A recent study reports the creation of an EA2 animal model by engineering a mouse line carrying the F1406C mutation in the orthologous mouse *Cacna1a* gene (Rose et al., 2014). It remains unclear, however, whether F1406C is associated with enhanced ERAD. Figure 7*A* shows that, compared with its WT counterpart, the F1406C mutant displays ~49% and ~26% reduction in protein expression in the absence and presence of auxiliary subunits, respectively, and that treatment with the proteasome inhibitor MG132 substantially ameliorates the mutant's protein expression deficit. Moreover, for both R1281X and F1406C, coexpression with RNF138 results in attenuation of protein level, whereas interfering with endogenous RNF138 function in HEK293T cells with RNF138-H36E leads to significantly enhanced protein expression (Fig. 7*B*). Similarly, shRNA suppression of endogenous RNF138 expression in HEK293T cells leads to a more than twofold increase in the EA2 mutants' protein levels (Fig. 7*C*).

Figure 8*A* demonstrates that the defective protein expression of R1281X and F1406C in HEK293T cells does not appear to result from a reduced mRNA level. Consistent with this notion, both R1281X and F1406C exhibit substantially accelerated turnover kinetics (protein half-life: ~1.6–2.2 h), which is effectively reversed in the presence of RNF138-H36E (protein half-life: ~6.0–8.3 h; Fig. 8*B*). As demonstrated by their dramatic upregu-

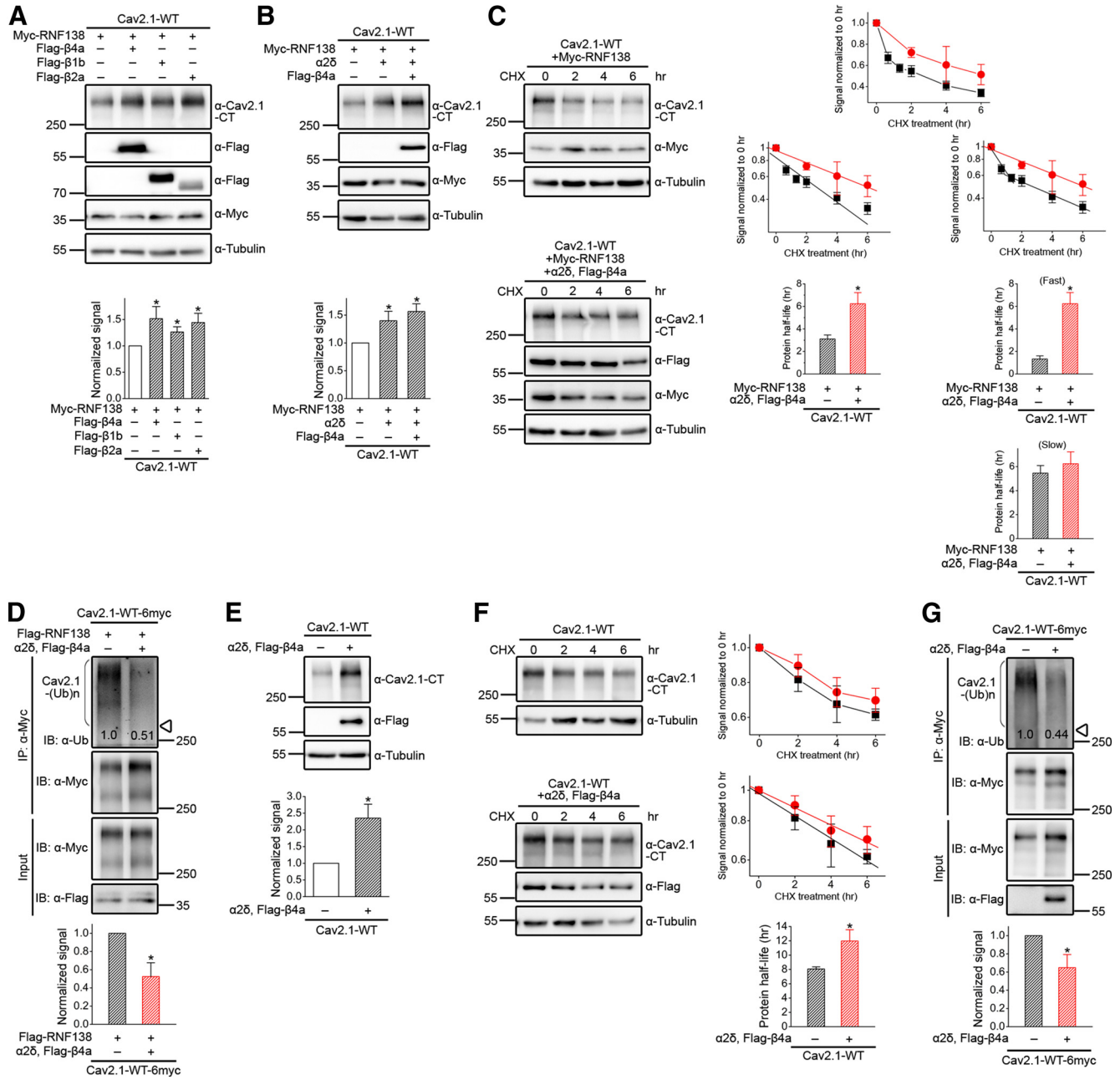

Figure 6. Auxiliary subunits protect $Ca_V2.1$ from RNF138-mediated protein degradation. ***A***, Effect of coexpression with Flag-tagged human β_{4a}, bovine β_{1b}, or bovine β_{2a} subunits on Myc-RNF138 regulation of $Ca_V2.1$ in HEK293T cells. Top, Representative immunoblots. Coexpression with the Flag vector was used as the control experiment. Bottom, Quantification of relative $Ca_V2.1$ protein level. Data were normalized to the Flag vector control ($n = 6–9$). ***B***, Effect of coexpression with human $\alpha_2\delta$ or $\alpha_2\delta$-β_{4a} subunits on Myc-RNF138 regulation of $Ca_V2.1$ protein level ($n = 7–9$). ***C***, Coexpression with auxiliary $\alpha_2\delta$ and β_{4a} subunits diminishes the effect of Myc-RNF138 on $Ca_V2.1$ turnover kinetics. The estimated $Ca_V2.1$ protein half-life value in the presence of Myc-RNF138 and auxiliary $\alpha_2\delta$ and β_{4a} subunits is ~6.2 ± 1.0 ($n = 8$; red) h. For comparison, also shown is the effect of Myc-RNF138 on $Ca_V2.1$ protein half-life in the absence of the auxiliary subunits (from Fig. 4*D*; black), which is subject to either single or double linear-regression analyses. ***D***, Coexpression with auxiliary $\alpha_2\delta$ and β_{4a} subunits attenuates the effect of Flag-RNF138 on $Ca_V2.1$ polyubiquitination ($n = 5$). In the presence of the auxiliary subunits, the mean relative value is 0.5 ± 0.2. ***E–G***, Effect of $\alpha_2\delta$ and β_{4a} subunits on $Ca_V2.1$ in HEK293T cells in the absence of Myc/Flag-RNF138 overexpression. ***E***, $\alpha_2\delta$-β_{4a} overexpression enhances $Ca_V2.1$ protein level ($n = 6$). ***F***, $\alpha_2\delta$-β_{4a} overexpression decelerates $Ca_V2.1$ turnover kinetics. The estimated $Ca_V2.1$ protein half-life values are ~8.1 ± 0.3 (with vector; $n = 7$; black) and 12.0 ± 1.6 (with $\alpha_2\delta$ and β_{4a}; $n = 5$; red) h. ***G***, $\alpha_2\delta$-β_{4a} overexpression reduces $Ca_V2.1$ polyubiquitination ($n = 5$). In the presence of the auxiliary subunits, the mean relative value is 0.7 ± 0.2. Open triangle refers to the expected location of the protein band corresponding to nonubiquitinated $Ca_V2.1$. $Ca_V2.1$, $\alpha_2\delta$, and β subunits were coexpressed in the molar ratio 1:2:1. Asterisks denote significant difference from the control (*$p < 0.05$).

lation in the presence of the lysine-less Ub-K0 (Fig. 8*C*), both EA2 mutants are subject to notable polyubiquitination. Figure 8*D* further illustrates that, compared with $Ca_V2.1$ WT, both R1281X and F1406C exhibit enhanced polyubiquitination, which can be further increased by RNF138, but is measurably diminished by RNF135-H36E. Together, these observations are consistent with the idea that RNF138 mediates enhanced ERAD of the two EA2-causing $Ca_V2.1$ mutants.

RNF138 controls functional expression of $Ca_V2.1$ channel

The foregoing investigation focuses on RNF138 regulation of $Ca_V2.1$ total protein level. An unanswered question is whether

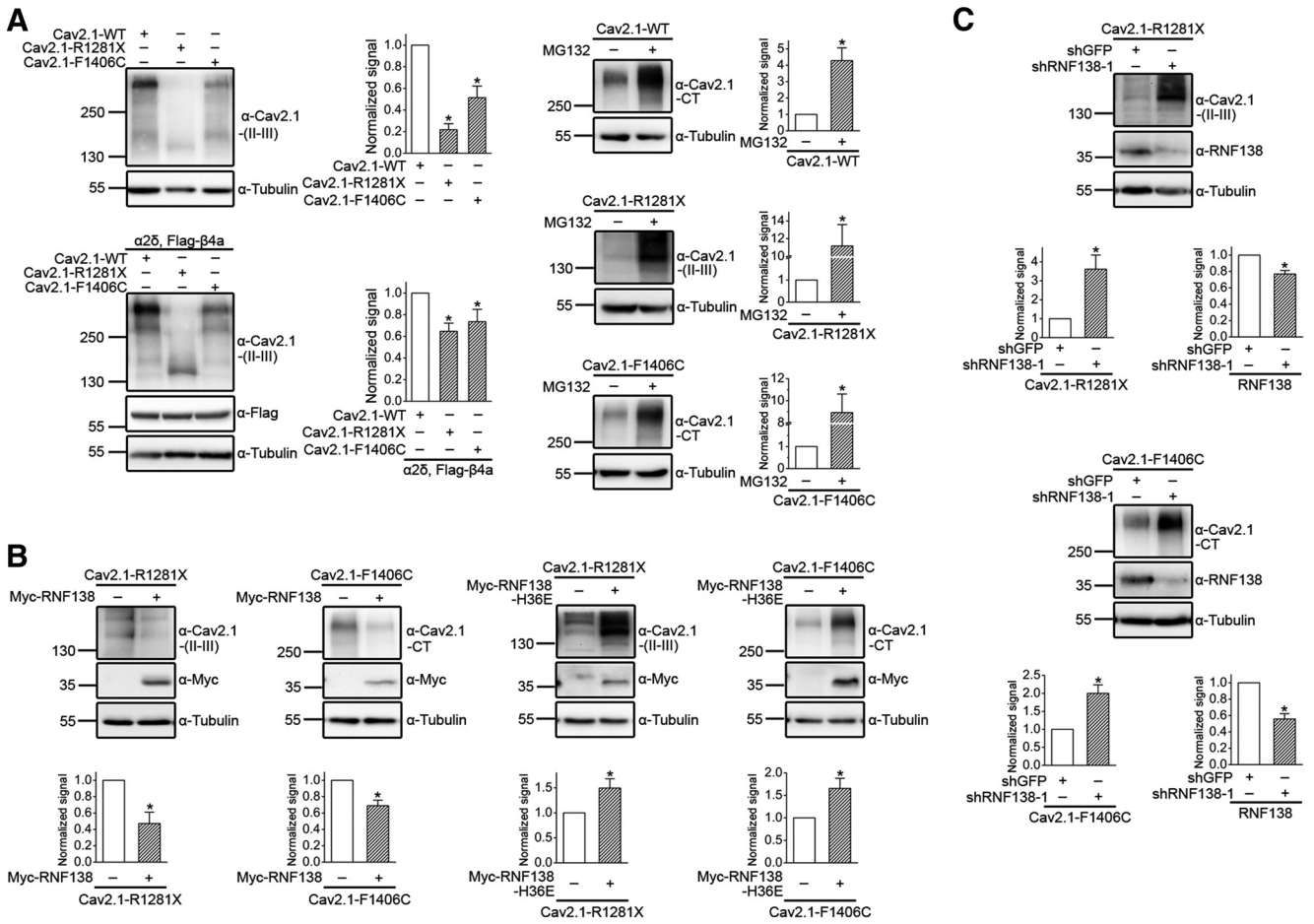

Figure 7. RNF138 regulates protein level of EA2-causing $Ca_V2.1$ mutants. ***A***, Left, Comparison of $Ca_V2.1$ WT and EA2 mutants (R1281X, F1406C) expression in HEK293T cells in the absence (top left) or presence (bottom left) of auxiliary $\alpha_2\delta$ and β_{4a} subunits. Immunoblotting of $Ca_V2.1$ proteins was performed with an antibody that recognizes the transmembrane domains II-III linker region of human $Ca_V2.1$ subunit [α-$Ca_V2.1$-(II–III)]. Relative $Ca_V2.1$ protein level was normalized to the corresponding WT control ($n = 7$). Right, Treatment with 10 μM MG132 for 24 h enhances protein level of EA2 mutants. $Ca_V2.1$ subunits were expressed in the absence of the auxiliary subunits. Data were normalized to the DMSO treatment (−) control ($n = 9–15$). ***B***, RNF138 (left) and the H36E mutant (right) regulate protein expression of EA2 mutants. Coexpression with the Myc vector was used as the control experiment. Data in each coexpression condition were normalized to the vector control ($n = 4–10$). ***C***, shRNA suppression of endogenous RNF138 expression in HEK293T cells increases protein level of EA2 mutants. Data were normalized to the shGFP infection control ($n = 4–8$). Asterisks denote significant difference from the control (*$p < 0.05$).

RNF138 may affect the membrane-trafficking property of $Ca_V2.1$ WT and EA2 mutants. To address this issue, we studied surface expression of $Ca_V2.1$ subunits in the presence of auxiliary $\alpha_2\delta$ and β_{4a} subunits by performing protein biotinylation assays. Figure 9*A* shows that the surface protein signal of R1281X and F1406C are only ~30% and ~58%, respectively, that of $Ca_V2.1$ WT. Moreover, the membrane-trafficking efficiency of the EA2 mutants, which was quantified by the ratio of surface expression to total protein level, is ~25% lower than that of their WT counterpart, consistent with our previous morphological evidence indicating that EA2 mutants are associated with defective membrane trafficking (Jeng et al., 2008). For $Ca_V2.1$ WT and the EA2 mutants, disrupting polyubiquitination with Ub-K0 does not significantly affect membrane trafficking efficiency (Fig. 9*B*). Similarly, coexpression with RNF138 (Fig. 9*C*) or RNF138-H36E (Fig. 9*D*) fails to detectably alter the membrane trafficking efficiency of $Ca_V2.1$ WT and EA2 mutants, suggesting that surface and total $Ca_V2.1$ protein levels are subject to comparable extents of RNF138-mediated suppression and that a significant fraction of the EA2 mutants protected from the ubiquitin–proteasome pathway by either Ub-K0 or RNF138-H36E is successfully exported from the ER to the plasma membrane.

We then examined the effect of RNF138 on functional expression of human $Ca_V2.1$ channels. Using the *Xenopus* oocyte system, we demonstrated that coexpression with RNF138 and RNF138-H36E results in considerable attenuation and enhancement, respectively, of Ba^{2+} current amplitudes through $Ca_V2.1$ channels (Fig. 10*A*,*B*). In contrast, RNF128 fails to affect $Ca_V2.1$ functional expression discernibly. We have shown previously that the F1406C mutant channel generates small but detectable Ba^{2+} currents in *Xenopus* oocytes (Jeng et al., 2006). Coexpression with RNF138 and the H36E mutant also significantly reduces and increases the functional expression of F1406C, respectively (Fig. 10*C*,*D*). The current amplitude of F1406C channel in the presence of RNF138-H36E, however, is still substantially smaller than that of $Ca_V2.1$ WT, which may be attributed to the mutant's defective membrane trafficking, as well as to a potential disruption of $Ca_V2.1$ biophysical properties imposed by the mutation at the pore region. The HEK293T expression system was also used for functional analyses of $Ca_V2.1$ WT channels (Fig. 10*E*,*F*). Consistent with our biochemical observations, enhancement of $Ca_V2.1$ polyubiquitination by coexpressing either ubiquitin or RNF138 notably diminishes whole-cell Ba^{2+} current density and a reverse ef-

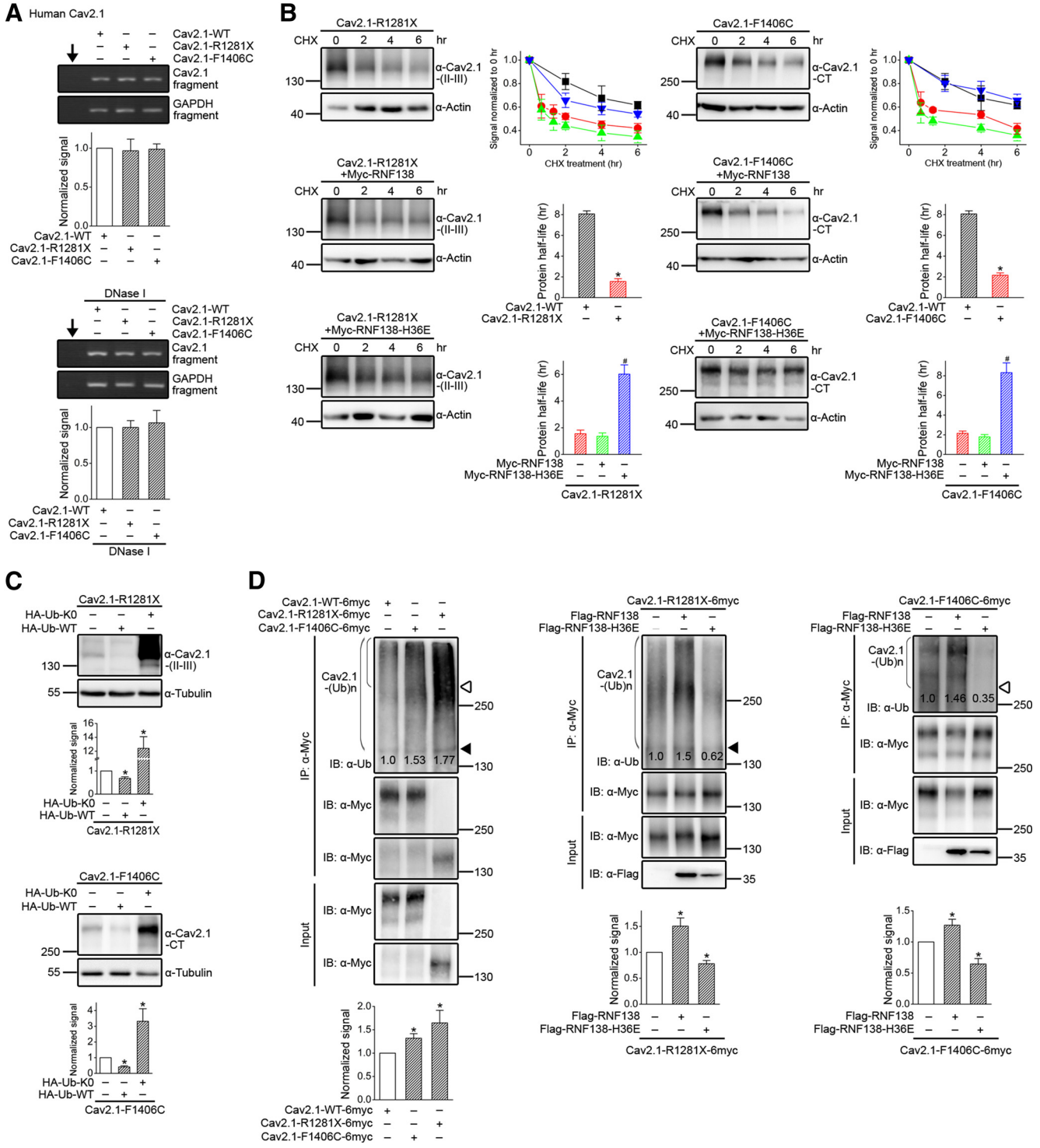

Figure 8. RNF138 mediates protein degradation of EA2 mutants. ***A***, Comparable mRNA levels for $Ca_V2.1$ WT, R1281X, and F1406C in HEK293T cells subject to the indicated transfection condition ($p > 0.05$; $n = 3$). RT-PCR was performed in the absence (top) or presence (bottom) of DNase I treatment before reverse transcription reaction. Vertical arrows refer to the blank control involving identical PCR in the absence of cDNA template. Standardized $Ca_V2.1$ signals were normalized with respect to $Ca_V2.1$ WT. ***B***, RNF138-H36E reverses the impaired protein stability of EA2 mutants. $Ca_V2.1$ subunits were expressed in the absence of auxiliary subunits. The estimated protein half-life values for R1281X are ~1.6 ± 0.3 h (with vector; $n = 7$; red), 1.4 ± 0.3 h (with RNF138; $n = 6$; green), and 6.0 ± 0.7 h (with RNF138-H36E; $n = 9$; blue). The estimated protein half-life values for F1406C are ~2.2 ± 0.2 h (with vector; $n = 7$; red), 1.8 ± 0.2 h (with RNF138; $n = 7$; green), and 8.3 ± 1.0 h (with RNF138-H36E; $n = 10$; blue). For comparison, also shown is the protein half-life value of $Ca_V2.1$ WT (with vector) from Figure 4*D* (black). ***C***, Coexpression with HA-Ub-K0 upregulates the protein level of EA2 mutants. Coexpression with the HA vector was used as the control experiment. The relative molar ratio to $Ca_V2.1$ is 1:1. Data were normalized to the HA vector control ($n = 5–8$). ***D***, EA2 mutants display enhanced polyubiquitination that is regulated by RNF138 ($n = 4–10$). Compared with $Ca_V2.1$ WT, the mean relative values are 1.7 ± 0.3 (R1281X) and 1.3 ± 0.1 (F1406C). For R1281X, the mean relative values are 1.5 ± 0.2 (with RNF138) and 0.8 ± 0.1 (with RNF138-H36E). For F1406C, the mean relative values are 1.3 ± 0.1 (with RNF138) and 0.7 ± 0.1 (with RNF138-H36E). Protein ubiquitination by endogenous ubiquitin in HEK293T cells was identified by immunoblotting with α-Ub. Open and filled triangles refer to the expected location of the protein band corresponding to nonubiquitinated $Ca_V2.1$ WT/F1406C and R1281X, respectively. Asterisks denote significant difference from the control (*$p < 0.05$).

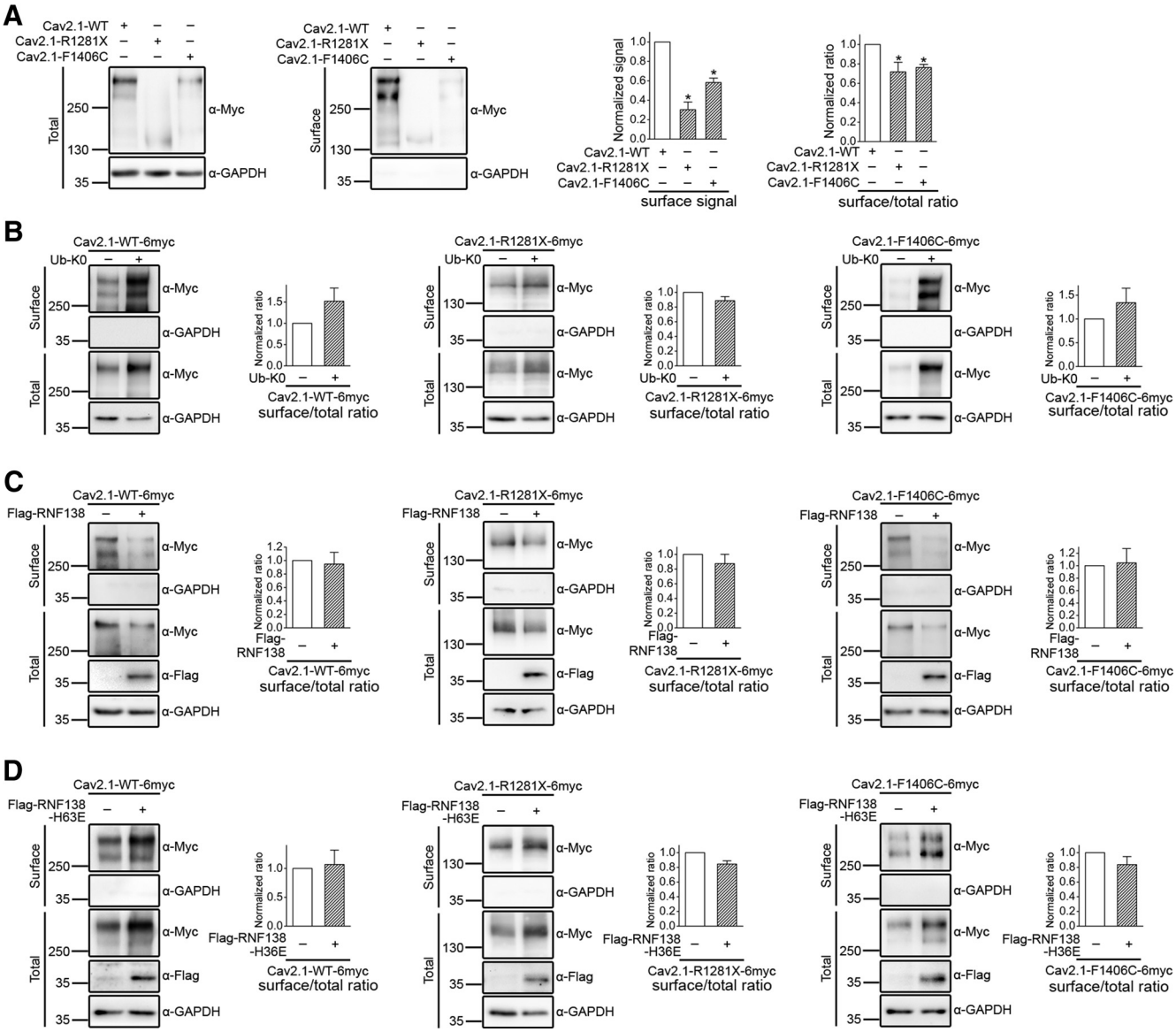

Figure 9. RNF138 attenuates surface expression of $Ca_V2.1$. ***A***, Surface biotinylation experiments on HEK293T cells expressing Myc-tagged $Ca_V2.1$ WT, R1281X, or F1406C ($Ca_V2.1$– 6myc). Left, Representative immunoblots. Cell lysates from biotinylated intact cells were either used directly for immunoblotting analyses (Total) or subject to streptavidin pull-down before immunoblotting analyses (Surface). $Ca_V2.1$– 6myc, $\alpha_2\delta$, and β_{4a} subunits were coexpressed in the molar ratio 1:2:1. GAPDH expression is displayed as the loading control. Right, Quantification of surface protein level (surface signal) and membrane trafficking efficiency (surface/total ratio; $n = 4$). The surface protein density was standardized as the ratio of surface signal to cognate total GAPDH signal, followed by normalization to that of $Ca_V2.1$-WT. The total protein density was standardized as the ratio of input signal to GAPDH signal. The membrane-trafficking efficiency was quantified as surface protein density divided by the corresponding standardized total protein density, followed by normalization to that of $Ca_V2.1$-WT. ***B***, Surface biotinylation experiments on HEK293T cells coexpressing $Ca_V2.1$– 6myc channel with HA-Ub-K0 ($n = 3$–8). Coexpression with the HA vector (−) was used as the control experiment. $Ca_V2.1$– 6myc and HA-Ub-K0 were coexpressed in the molar ratio 1:1. ***C***, ***D***, Surface biotinylation experiments on HEK293T cells coexpressing $Ca_V2.1$– 6myc channel with Flag-RNF138 ($n = 4$) or Flag-RNF138-H36E ($n = 3$–6). Coexpression with the Flag vector (−) was used as the control experiment. $Ca_V2.1$– 6myc and Flag-RNF138 were coexpressed in the molar ratio 1:3. Asterisks denote significant difference from the control ($^*p < 0.05$).

fect on $Ca_V2.1$ functional expression was found in the presence of Ub-K0 or RNF138-H36E.

RNF138 contributes to the dominant-negative effect of EA2 mutants on $Ca_V2.1$ WT

Upon coexpressing with their WT counterpart, both R1281X and F1406C mutants are known to exert significant dominant-negative effects on functional expression of $Ca_V2.1$ WT channels (Jeng et al., 2006; Jeng et al., 2008). In addition, R1281X has been shown to elicit prominent proteasomal degradation of $Ca_V2.1$ WT subunits (Mezghrani et al., 2008). Whether the missense mutant F1406C may instigate enhanced degradation of $Ca_V2.1$ WT is still unclear. Moreover, a key question that we need to address here is whether EA2 mutant-induced protein degradation of $Ca_V2.1$ WT subunit is also mediated by RNF138, or rather by an as yet unidentified E3 ubiquitin ligase. Figure 11*A* shows that, in the presence of auxiliary $\alpha_2\delta$ and β_{4a} subunits, equimolar coexpression with R1281X or F1406C results in an ~34–75% reduction in the total protein level of $Ca_V2.1$ WT subunits in HEK293T cells. These suppression effects can be effectively reversed by treatment with the proteasome inhibitor MG132 (Fig. 11*B*), as well as by coexpression with RNF138-H36E (Fig. 11*C*). Figure 11*D* further illustrates that, in the presence of either R1281X or F1406C, the protein half-life of $Ca_V2.1$ WT substantially decreases from ~8 h to ~2 h. Upon coexpression with RNF138-H36E, however, the turnover kinetics of $Ca_V2.1$ WT

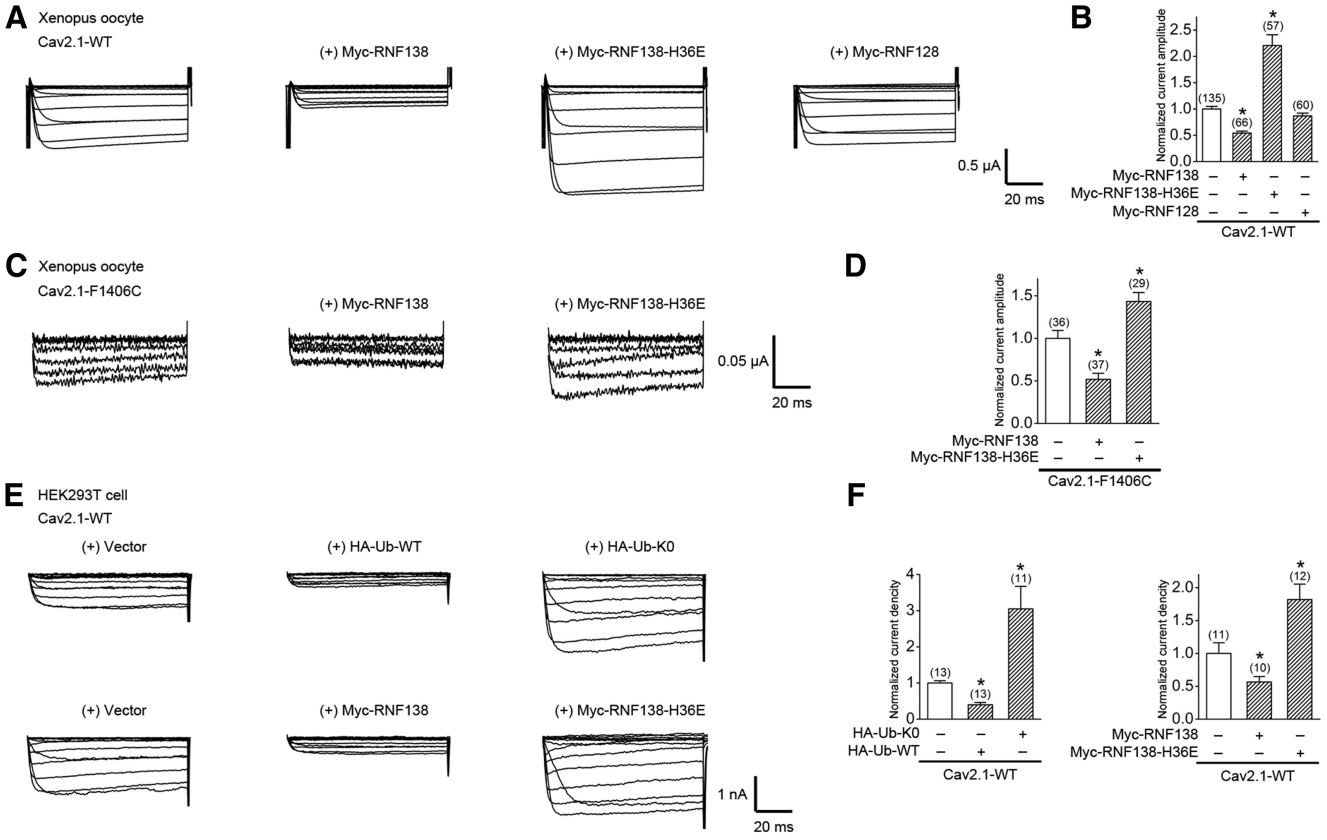

Figure 10. RNF138 suppresses functional expression of $Ca_V2.1$. Representative Ba^{2+} current traces through $Ca_V2.1$ WT (***A***, ***B***) and F1406C (***C***, ***D***) channels under different coexpression conditions in *Xenopus* oocytes are shown. The holding potential was −90 mV and 70 ms test pulses ranged from −80 mV to +60 mV in +10 mV steps. The peak Ba^{2+} current values at +20 mV were measured for comparing relative current amplitudes. Data were normalized to the corresponding water coinjection control. ***E***, ***F***, Representative Ba^{2+} current traces through $Ca_V2.1$ WT channels under different coexpression conditions in HEK293T cells. The peak Ba^{2+} current amplitudes at +10 mV were measured for comparing relative current densities. Data were normalized to the corresponding vector control. $Ca_V2.1$, $\alpha_2\delta$, and β_{4a} subunits were coexpressed in the molar ratio 1:2:2. The number of observation is shown in parentheses. Asterisks denote a significant difference from the control condition ($^*p < 0.05$).

remains practically unchanged in the absence or presence of the EA2 mutants (protein half-life: ~9–10 h). These findings strongly suggest that RNF138 indeed contributes to EA2 mutant-induced proteasomal degradation of $Ca_V2.1$ WT subunits.

We then investigated whether coexpression with RNF138-H36E may also reverse the dominant-negative effect of EA2 mutants on functional expression of human $Ca_V2.1$ WT channels. Figure 11*E* shows that coexpression with RNF138-H36E only partially restores the impaired $Ca_V2.1$ WT current amplitudes, which is in direct contrast to the foregoing biochemical observations that RNF138-H36E virtually eradicates the EA2 mutant-induced deficit in $Ca_V2.1$ WT protein expression. Previous confocal microscopic evidence from us and others suggests that coexpression with R1281X induces significant ER retention of $Ca_V2.1$ WT subunits (Jeng et al., 2008; Mezghrani et al., 2008). In agreement with this notion, surface biotinylation analyses reveal that coexpression with the EA2 mutants decreases the membrane trafficking efficiency of $Ca_V2.1$ WT by ~32–54% (Fig. 11*F*). Figure 11*F* further demonstrates that, in the presence of RNF138-H36E, the EA2 mutants still induce an attenuation of $Ca_V2.1$ WT-trafficking efficiency by ~25–51%, which may in part explain why RNF138-H36E fails to completely reverse the dominant-negative inhibition of $Ca_V2.1$ WT current expression.

Discussion

After being recognized by the ER quality control system, misfolded protein is subject to ubiquitination by the concerted activity of three enzymes: the E1 ubiquitin-activating enzyme, the E2 ubiquitin-conjugating enzyme, and the E3 ubiquitin ligase (Hebert and Molinari, 2007; Vembar and Brodsky, 2008; Claessen et al., 2012; Kleiger and Mayor, 2014). In higher eukaryotes, there are >1000 different E3 ligases that can be divided into two major families: the homologous to E6-AP C terminus (HECT) family and the RING family (Deshaies and Joazeiro, 2009; Rotin and Kumar, 2009; MacGurn et al., 2012). Furthermore, >600 distinct RING finger E3 ligases are estimated to express in human cells.

To the best of our knowledge, of the 10 subfamilies of Ca_V $\alpha1$ subunits, to date, only the E3 ligase for $Ca_V1.2$ (the RING finger protein RFP2) has been recognized (Altier et al., 2011). Here, we set out to delineate the protein degradation mechanism of human $Ca_V2.1$ subunit by identifying its E3 ubiquitin ligase. Our data suggest that misfolded $Ca_V2.1$ protein in the ER goes through polyubiquitination before being targeted for proteasomal degradation. Covalent linkage of ubiquitin molecules to $Ca_V2.1$ is mediated by the RING finger protein RNF138 that is physically associated and subcellularly colocalized with $Ca_V2.1$ in neurons. Disrupting endogenous RNF138 function with RNF138-H36E, hRNF138-ΔN, or shRNA infection significantly upregulates the $Ca_V2.1$ protein level and enhances $Ca_V2.1$ protein stability. The control of $Ca_V2.1$ protein expression by RNF138 appears to be quite specific in that overexpressing the E3 ligase fails to change the protein level of $Ca_V1.2$ and $Ca_V2.2$ measurably. In agreement

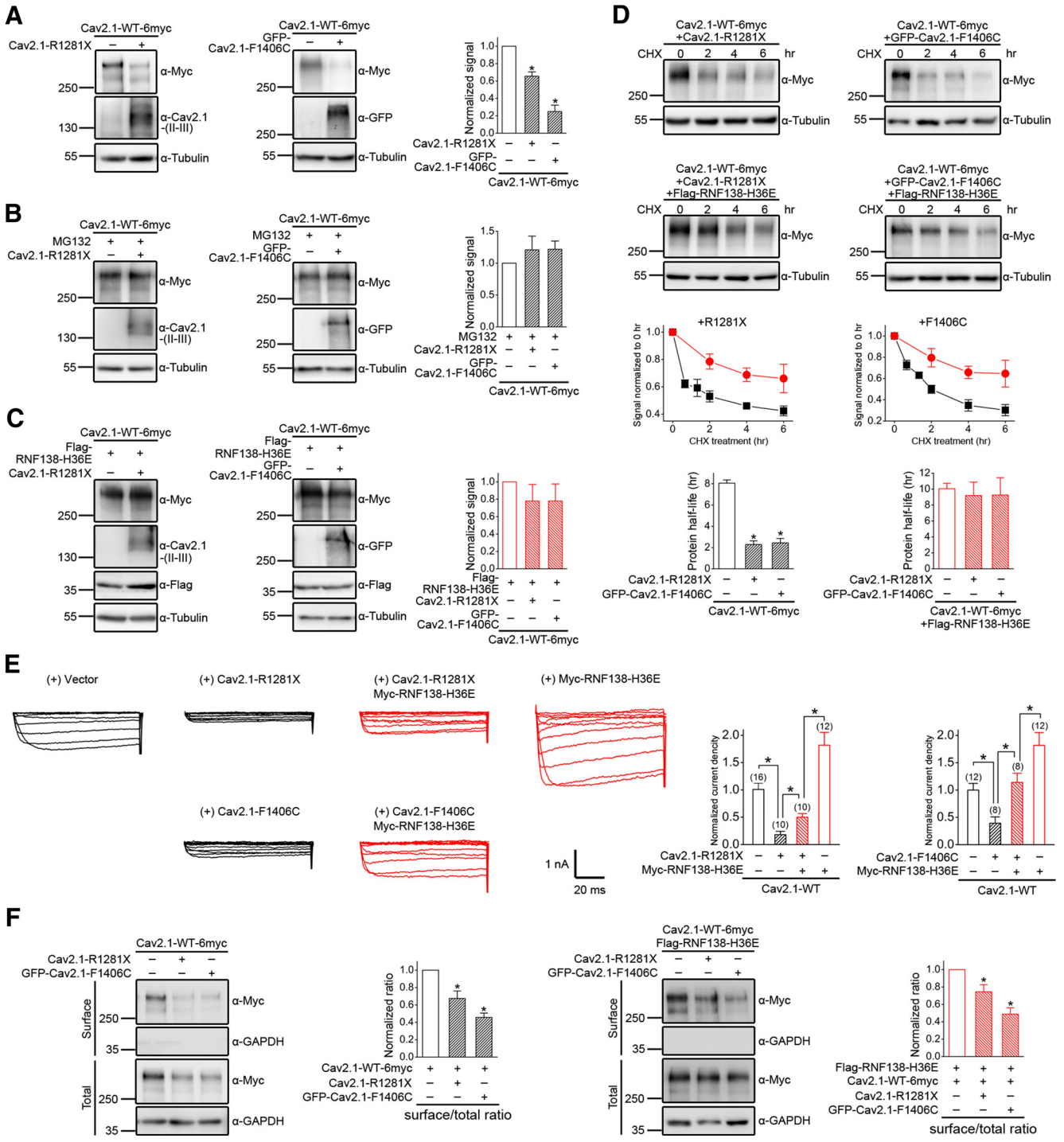

Figure 11. RNF138 promotes EA2 mutant-induced degradation of $Ca_V2.1$ WT subunits. ***A***, Biochemical demonstration of the dominant-negative effect of untagged R1281X and GFP-tagged F1406C on $Ca_V2.1$-WT-6myc protein expression ($n = 4–8$). EA2 mutant was coexpressed with $Ca_V2.1$-WT in HEK293T cells in the molar ratio 1:1. Auxiliary $\alpha_2\delta$ and β_{4a} subunits were also coexpressed together. ***B***, Treatment with 10 μM MG132 for 24 h fully reverses the dominant-negative effect of EA2 mutants on $Ca_V2.1$-WT-6myc protein expression ($n = 5–7$). ***C***, Coexpression with RNF138-H36E fully reverses the dominant-negative effect of EA2 mutants on $Ca_V2.1$-WT-6myc protein expression ($n = 4–5$). Quantitative data collected in the presence of RNF138-H36E are illustrated in red. ***D***, Coexpression with RNF138-H36E reverses the dominant-negative effect of EA2 mutants on $Ca_V2.1$-WT-6myc turnover kinetics. The estimated protein half-life values for $Ca_V2.1$-WT-6myc in the absence of RNF138-H36E (black) are $\sim 8.1 \pm 0.3$ h (with vector; $n = 9$), 2.3 ± 0.4 h (with R1281X; $n = 7$), and 2.4 ± 0.4 h (with F1406C; $n = 10$). The estimated protein half-life values for $Ca_V2.1$-WT-6myc in the presence of RNF138-H36E (red) are $\sim 10.1 \pm 0.7$ h (with vector; $n = 6$), 9.2 ± 1.7 h (with R1281X; $n = 5$), and 9.3 ± 2.2 h (with F1406C; $n = 5$). ***E***, Coexpression with RNF138-H36E partially reverses the dominant-negative effect of EA2 mutants on $Ca_V2.1$ WT current density. The number of observations is shown in parentheses. ***F***, Biotinylation analyses of the dominant-negative effect of EA2 mutants on $Ca_V2.1$ WT membrane trafficking in the absence (left) or presence (right) of RNF138-H36E. Asterisks denote significant difference from the control ($^*p < 0.05$).

with previously demonstrated role of auxiliary $\alpha_2\delta$ and β subunits in facilitating forward trafficking and preventing protein degradation of Ca_V α_1 subunits, respectively (Cantí et al., 2005; Altier et al., 2011; Waithe et al., 2011; Page et al., 2016), coexpression with the auxiliary subunits significantly diminishes RNF138-mediated $Ca_V2.1$ polyubiquitination and degradation. Moreover, RNF138 specifically regulates $Ca_V2.1$ protein turnover kinetics without discernibly affecting the Ca^{2+} channel's membrane trafficking property. Overall, we pro-

pose that RNF138 plays a critical role in the homeostatic regulation of $Ca_V2.1$ protein level and functional expression in neurons.

In both the central and peripheral nervous systems, $Ca_V2.1$ channels are essential in controlling presynaptic neurotransmitter release; in the brain, $Ca_V2.1$ channels also play a critical role in postsynaptic neurons by regulating dendritic Ca^{2+} transients and dendrosomatic excitability (Pietrobon, 2010; Catterall, 2011; Higley and Sabatini, 2012). Emerging evidence suggests that ubiquitin-mediated proteolysis modulates key proteins at both presynaptic terminals and postsynaptic compartments (Tai and Schuman, 2008; Tsai, 2014). For example, the E3 ubiquitin ligase UBE3A (also known as E6-AP) controls synaptic strength and synapse development via ubiquitination of the postsynaptic signaling protein Arc (Greer et al., 2010; Kühnle et al., 2013; Mabb et al., 2014). Furthermore, ionotropic glutamate receptor subunit A2 is regulated by E3 ubiquitin ligases Nedd4–1 and RNF167 in a neuronal activity-dependent manner (Schwarz et al., 2010; Lussier et al., 2011; Lussier et al., 2012). Interestingly, both our biochemical and morphological evidence supports the idea that $Ca_V2.1$ and RNF138 colocalize at synaptic regions in the rat brain (Fig. 2). It remains to be determined in the future whether RNF138-mediated regulation of $Ca_V2.1$ protein level and functional expression may play a significant role in modulating presynaptic and postsynaptic neuronal activities in the brain.

A substrate protein may be subject to regulation by more than one type of E3 ligase; for instance, at least seven distinct types of E3 ligase appear to contribute to the ubiquitination of the human Cl-channel cystic fibrosis transmembrane conductance regulator (CFTR; Lukacs and Verkman, 2012; Pranke and Sermet-Gaudelus, 2014). Therefore, in theory, there is a possibility that $Ca_V2.1$ WT and EA2 mutants, as well as EA2 mutant-induced enhanced degradation of $Ca_V2.1$ WT, may be differentially regulated by distinct E3 ubiquitin ligases. Our biochemical analyses reveal that the impaired protein stability of R1281X and F1406C is effectively rescued by interrupting endogenous RNF138 function with shRNA infection or RNF138-H36E overexpression (Figs. 7, 8), suggesting that RNF138 also mediates the ubiquitin–proteasome pathway of the two EA2 mutants. In addition, if the dominant-negative effect of the EA2 mutants is promoted by a different E3 ligase, then one would expect that rescuing $Ca_V2.1$ WT and EA2 mutant protein expression with RNF138-H36E should not affect EA2 mutant-induced aberrant degradation of $Ca_V2.1$ WT detectably, which is quite opposite to what we present in Figure 11. Therefore, as far as EA2 is concerned, we propose that RNF138 serves as the primary E3 ubiquitin ligase promoting the pathogenic degradation of human $Ca_V2.1$ subunits.

Accumulating evidence indicates that the dominant-negative effect of EA2-causing N-terminal truncation mutants involves direct interaction between an N-terminal region of the mutants and an as yet unidentified region of $Ca_V2.1$ WT subunit, which in turn induces protein misfolding, ER retention, and therefore enhanced proteasomal degradation of the WT subunit (Mezghrani et al., 2008; Page et al., 2010; Dahimene et al., 2016). In this study, we demonstrate that, in addition to enhanced protein degradation, both the truncation mutant R1281X and the full-length mutant F1406C are associated with defective membrane trafficking that cannot be reversed by blocking protein degradation (Fig. 9). A similar lack of improvement in surface expression in response to proteasome inhibition was also reported previously for a mutant $Ca_V2.2$ subunit associated with reduced protein expression (Waithe et al., 2011), suggesting that these mutant $Ca_V2.1$/2.2 subunits are endowed with protein misfolding that perturbs cell surface trafficking. We further confirm here that the EA2 mutants also disrupt membrane trafficking of $Ca_V2.1$ WT, which appears to be reversed efficiently by low-temperature incubation (Jeng et al., 2008), but not by coexpression with RNF138-H36E (Fig. 11). Nevertheless, blocking protein degradation also does not seem to exacerbate the EA2 mutant-induced membrane trafficking defect of $Ca_V2.1$ WT (Fig. 11). Together, these observations suggest that a significant fraction of the misfolded $Ca_V2.1$ WT subunits spared from proteasomal degradation may still be properly exported to the plasma membrane; otherwise, their membrane trafficking efficiency would have been substantially reduced in the presence of RNF138-H36E. At present, the mechanistic significance of this inference is still an open question. It may imply that some of the spared $Ca_V2.1$ WT subunits are somehow successfully refolded by molecular chaperones in the ER. Alternatively, one can also argue that defective membrane trafficking and impaired protein stability may represent two related, but independent, consequences of EA2 mutant-induced misfolding of $Ca_V2.1$ WT subunits; therefore, the membrane trafficking efficiency of $Ca_V2.1$ WT, albeit defective, remains approximately constant regardless of the extent of their aberrant degradation. Further structural investigations are required to address these issues.

Here, we identify RNF138 as the E3 ubiquitin ligase promoting EA2-associated aberrant degradation of human $Ca_V2.1$ protein. Moreover, we demonstrate that specific interruption of endogenous RNF138 function effectively recovers $Ca_V2.1$ protein level. Nonetheless, blocking protein degradation is insufficient to reverse EA2 mutant-induced suppression of $Ca_V2.1$ WT current level fully. A recent study reports the first application of a peptide derived from N-terminal sequences of EA2 truncation mutants in disrupting the dominant-negative interaction of the truncation mutants, which, however, only leads to partial restoration of the functional expression of Ca_V2 channels (Dahimene et al., 2016). In both cases, the lack of complete functional recovery may be attributed to the foregoing membrane-trafficking deficit of $Ca_V2.1$ WT induced by EA2 mutants because functional expression is determined by both total protein level and membrane trafficking efficiency. The disease-causing CFTR ΔF508 mutant is associated with severely impaired membrane trafficking that results in a virtual loss of functional expression and application of low temperature or chemical compounds is known to correct the CFTR mutant's membrane-trafficking defect successfully, thereby restoring its Cl-transport function; in fact, several chemical compounds are being carefully evaluated for their clinical potentials as pharmacological chaperones (Birault et al., 2013; Pranke and Sermet-Gaudelus, 2014). Therefore, it will be essential in the future to search for novel chemical chaperones capable of correcting membrane trafficking of $Ca_V2.1$. Overall, the present study provides a proof of concept that preventing excessive $Ca_V2.1$ degradation with RNF138 blockers, disrupting the deleterious $Ca_V2.1$ intermolecular interaction with specific N-terminal peptides, as well as facilitating $Ca_V2.1$ membrane trafficking with pharmacological chaperones may together pave the way for future development of novel therapeutic strategies aimed at alleviating the neurological disorders associated with patients suffering from EA2.

References

Abriel H, Staub O (2005) Ubiquitylation of ion channels. Physiology (Bethesda) 20:398–407. CrossRef Medline

Adams PJ, Garcia E, David LS, Mulatz KJ, Spacey SD, Snutch TP (2009) Ca(V)2.1 P/Q-type calcium channel alternative splicing affects the functional impact of familial hemiplegic migraine mutations: implications for calcium channelopathies. Channels (Austin) 3:110–121. CrossRef Medline

Altier C, Garcia-Caballero A, Simms B, You H, Chen L, Walcher J, Tedford

HW, Hermosilla T, Zamponi GW (2011) The Cavbeta subunit prevents RFP2-mediated ubiquitination and proteasomal degradation of L-type channels. Nat Neurosci 14:173–180. CrossRef Medline

Anderson TW, Wright C, Brooks WS (2010) The E3 ubiquitin ligase NARF promotes colony formation in vitro and exhibits enhanced expression levels in glioblastoma multiforme in vivo. American Journal of Undergraduate Research 9:23–30.

Baloh RW (2012) Episodic ataxias 1 and 2. Handb Clin Neurol 103:595–602. CrossRef Medline

Banker G, Goslin K (1998) Culturing nerve cells, Ed 2. Cambridge, MA: MIT.

Birault V, Solari R, Hanrahan J, Thomas DY (2013) Correctors of the basic trafficking defect of the mutant F508del-CFTR that causes cystic fibrosis. Curr Opin Chem Biol 17:353–360. CrossRef Medline

Bloom J, Amador V, Bartolini F, DeMartino G, Pagano M (2003) Proteasome-mediated degradation of p21 via N-terminal ubiquitinylation. Cell 115:71–82. CrossRef Medline

Brooks WS, Banerjee S, Crawford DF (2014) RNF138/NARF is a cell cycle regulated E3 ligase that polyubiquitinates G2E3. JSM Cell Dev Biol 2:1005.

Cahill AL, Hurley JH, Fox AP (2000) Coexpression of cloned alpha(1B), beta(2a), and alpha(2)/delta subunits produces non-inactivating calcium currents similar to those found in bovine chromaffin cells. J Neurosci 20:1685–1693. Medline

Cantí C, Nieto-Rostro M, Foucault I, Heblich F, Wratten J, Richards MW, Hendrich J, Douglas L, Page KM, Davies A, Dolphin AC (2005) The metal-ion-dependent adhesion site in the Von Willebrand factor-A domain of alpha2delta subunits is key to trafficking voltage-gated Ca2+ channels. Proc Natl Acad Sci U S A 102:11230–11235. CrossRef Medline

Catterall WA (2000) Structure and regulation of voltage-gated Ca2+ channels. Annu Rev Cell Dev Biol 16:521–555. CrossRef Medline

Catterall WA (2011) Voltage-gated calcium channels. Cold Spring Harb Perspect Biol 3:a003947. CrossRef Medline

Catterall WA, Perez-Reyes E, Snutch TP, Striessnig J (2005) International Union of Pharmacology. XLVIII. Nomenclature and structure-function relationships of voltage-gated calcium channels. Pharmacol Rev 57:411–425. CrossRef Medline

Chen Y, Deng L, Maeno-Hikichi Y, Lai M, Chang S, Chen G, Zhang JF (2003) Formation of an endophilin-Ca2+ channel complex is critical for clathrin-mediated synaptic vesicle endocytosis. Cell 115:37–48. CrossRef Medline

Claessen JH, Kundrat L, Ploegh HL (2012) Protein quality control in the ER: balancing the ubiquitin checkbook. Trends Cell Biol 22:22–32. CrossRef Medline

Dahimene S, Page KM, Nieto-Rostro M, Pratt WS, D'Arco M, Dolphin AC (2016) A CaV2.1 N-terminal fragment relieves the dominant-negative inhibition by an Episodic ataxia 2 mutant. Neurobiol Dis 93:243–256. CrossRef Medline

Deshaies RJ, Joazeiro CA (2009) RING domain E3 ubiquitin ligases. Annu Rev Biochem 78:399–434. CrossRef Medline

Graves TD, Imbrici P, Kors EE, Terwindt GM, Eunson LH, Frants RR, Haan J, Ferrari MD, Goadsby PJ, Hanna MG, van den Maagdenberg AM, Kullmann DM (2008) Premature stop codons in a facilitating EF-hand splice variant of CaV2.1 cause episodic ataxia type 2. Neurobiol Dis 32:10–15. CrossRef Medline

Greer PL, Hanayama R, Bloodgood BL, Mardinly AR, Lipton DM, Flavell SW, Kim TK, Griffith EC, Waldon Z, Maehr R, Ploegh HL, Chowdhury S, Worley PF, Steen J, Greenberg ME (2010) The Angelman Syndrome protein Ube3A regulates synapse development by ubiquitinating arc. Cell 140:704–716. CrossRef Medline

Hebert DN, Molinari M (2007) In and out of the ER: protein folding, quality control, degradation, and related human diseases. Physiol Rev 87:1377–1408. CrossRef Medline

Higley MJ, Sabatini BL (2012) Calcium signaling in dendritic spines. Cold Spring Harb Perspect Biol 4:a005686. CrossRef Medline

Holderith N, Lorincz A, Katona G, Rózsa B, Kulik A, Watanabe M, Nusser Z (2012) Release probability of hippocampal glutamatergic terminals scales with the size of the active zone. Nat Neurosci 15:988–997. CrossRef Medline

Hoppa MB, Lana B, Margas W, Dolphin AC, Ryan TA (2012) alpha2delta expression sets presynaptic calcium channel abundance and release probability. Nature 486:122–125. CrossRef Medline

Jen JC, Graves TD, Hess EJ, Hanna MG, Griggs RC, Baloh RW, Baloh RW (2007) Primary episodic ataxias: diagnosis, pathogenesis and treatment. Brain 130:2484–2493. CrossRef Medline

Jen J, Wan J, Graves M, Yu H, Mock AF, Coulin CJ, Kim G, Yue Q, Papazian DM, Baloh RW (2001) Loss-of-function EA2 mutations are associated with impaired neuromuscular transmission. Neurology 57:1843–1848. CrossRef Medline

Jen J, Kim GW, Baloh RW (2004) Clinical spectrum of episodic ataxia type 2. Neurology 62:17–22. CrossRef Medline

Jeng CJ, Chen YT, Chen YW, Tang CY (2006) Dominant-negative effects of human P/Q-type Ca2+ channel mutations associated with episodic ataxia type 2. Am J Physiol Cell Physiol 290:C1209–C1220. Medline

Jeng CJ, Sun MC, Chen YW, Tang CY (2008) Dominant-negative effects of episodic ataxia type 2 mutations involve disruption of membrane trafficking of human P/Q-type Ca2+ channels. J Cell Physiol 214:422–433. CrossRef Medline

Jouvenceau A, Eunson LH, Spauschus A, Ramesh V, Zuberi SM, Kullmann DM, Hanna MG (2001) Human epilepsy associated with dysfunction of the brain P/Q-type calcium channel. Lancet 358:801–807. CrossRef Medline

Kaeser PS, Deng L, Wang Y, Dulubova I, Liu X, Rizo J, Südhof TC (2011) RIM proteins tether Ca2+ channels to presynaptic active zones via a direct PDZ-domain interaction. Cell 144:282–295. CrossRef Medline

Kim JH, Park SM, Kang MR, Oh SY, Lee TH, Muller MT, Chung IK (2005) Ubiquitin ligase MKRN1 modulates telomere length homeostasis through a proteolysis of hTERT. Genes Dev 19:776–781. CrossRef Medline

Kleiger G, Mayor T (2014) Perilous journey: a tour of the ubiquitin–proteasome system. Trends Cell Biol 24:352–359. CrossRef Medline

Koester HJ, Sakmann B (2000) Calcium dynamics associated with action potentials in single nerve terminals of pyramidal cells in layer 2/3 of the young rat neocortex. J Physiol 529:625–646. CrossRef Medline

Kravtsova-Ivantsiv Y, Ciechanover A (2012) Non-canonical ubiquitin-based signals for proteasomal degradation. J Cell Sci 125:539–548. CrossRef Medline

Kühnle S, Mothes B, Matentzoglu K, Scheffner M (2013) Role of the ubiquitin ligase E6AP/UBE3A in controlling levels of the synaptic protein Arc. Proc Natl Acad Sci U S A 110:8888–8893. CrossRef Medline

Kulik A, Nakadate K, Hagiwara A, Fukazawa Y, Luján R, Saito H, Suzuki N, Futatsugi A, Mikoshiba K, Frotscher M, Shigemoto R (2004) Immunocytochemical localization of the alpha 1A subunit of the P/Q-type calcium channel in the rat cerebellum. Eur J Neurosci 19:2169–2178. CrossRef Medline

Lee A, Westenbroek RE, Haeseleer F, Palczewski K, Scheuer T, Catterall WA (2002) Differential modulation of Ca(v)2.1 channels by calmodulin and Ca2+-binding protein 1. Nat Neurosci 5:210–217. CrossRef Medline

Lineberry N, Su L, Soares L, Fathman CG (2008) The single subunit transmembrane E3 ligase gene related to anergy in lymphocytes (GRAIL) captures and then ubiquitinates transmembrane proteins across the cell membrane. J Biol Chem 283:28497–28505. CrossRef Medline

Lipscombe D, Allen SE, Toro CP (2013) Control of neuronal voltage-gated calcium ion channels from RNA to protein. Trends Neurosci 36:598–609. CrossRef Medline

Long P, Samnakay P, Jenner P, Rose S (2012) A yeast two-hybrid screen reveals that osteopontin associates with MAP1A and MAP1B in addition to other proteins linked to microtubule stability, apoptosis and protein degradation in the human brain. Eur J Neurosci 36:2733–2742. CrossRef Medline

Lukacs GL, Verkman AS (2012) CFTR: folding, misfolding and correcting the DeltaF508 conformational defect. Trends Mol Med 18:81–91. CrossRef Medline

Lussier MP, Nasu-Nishimura Y, Roche KW (2011) Activity-dependent ubiquitination of the AMPA receptor subunit GluA2. J Neurosci 31:3077–3081. CrossRef Medline

Lussier MP, Herring BE, Nasu-Nishimura Y, Neutzner A, Karbowski M, Youle RJ, Nicoll RA, Roche KW (2012) Ubiquitin ligase RNF167 regulates AMPA receptor-mediated synaptic transmission. Proc Natl Acad Sci U S A 109:19426–19431. CrossRef Medline

Mabb AM, Je HS, Wall MJ, Robinson CG, Larsen RS, Qiang Y, Corrêa SA, Ehlers MD (2014) Triad3A regulates synaptic strength by ubiquitination of Arc. Neuron 82:1299–1316. CrossRef Medline

MacGurn JA, Hsu PC, Emr SD (2012) Ubiquitin and membrane protein

turnover: from cradle to grave. Annu Rev Biochem 81:231–259. CrossRef Medline

Mantuano E, Romano S, Veneziano L, Gellera C, Castellotti B, Caimi S, Testa D, Estienne M, Zorzi G, Bugiani M, Rajabally YA, Barcina MJ, Servidei S, Panico A, Frontali M, Mariotti C (2010) Identification of novel and recurrent CACNA1A gene mutations in fifteen patients with episodic ataxia type 2. J Neurol Sci 291:30–36. CrossRef Medline

Mezghrani A, Monteil A, Watschinger K, Sinnegger-Brauns MJ, Barrère C, Bourinet E, Nargeot J, Striessnig J, Lory P (2008) A destructive interaction mechanism accounts for dominant-negative effects of misfolded mutants of voltage-gated calcium channels. J Neurosci 28:4501–4511. CrossRef Medline

Nachbauer W, Nocker M, Karner E, Stankovic I, Unterberger I, Eigentler A, Schneider R, Poewe W, Delazer M, Boesch S (2014) Episodic ataxia type 2: phenotype characteristics of a novel CACNA1A mutation and review of the literature. J Neurol 261:983–991. CrossRef Medline

Obermair GJ, Szabo Z, Bourinet E, Flucher BE (2004) Differential targeting of the L-type Ca2+ channel alpha 1C (CaV1.2) to synaptic and extrasynaptic compartments in hippocampal neurons. Eur J Neurosci 19:2109–2122. CrossRef Medline

Page KM, Heblich F, Davies A, Butcher AJ, Leroy J, Bertaso F, Pratt WS, Dolphin AC (2004) Dominant-negative calcium channel suppression by truncated constructs involves a kinase implicated in the unfolded protein response. J Neurosci 24:5400–5409. CrossRef Medline

Page KM, Heblich F, Margas W, Pratt WS, Nieto-Rostro M, Chaggar K, Sandhu K, Davies A, Dolphin AC (2010) N terminus is key to the dominant negative suppression of Ca(V)2 calcium channels: implications for episodic ataxia type 2. J Biol Chem 285:835–844. CrossRef Medline

Page KM, Rothwell SW, Dolphin AC (2016) The CaVbeta subunit protects the I-II loop of the voltage-gated calcium channel CaV2.2 from proteasomal degradation but not oligoubiquitination. J Biol Chem 291:20402–20416. CrossRef Medline

Pietrobon D (2010) CaV2.1 channelopathies. Pflugers Arch 460:375–393. CrossRef Medline

Pranke IM, Sermet-Gaudelus I (2014) Biosynthesis of cystic fibrosis transmembrane conductance regulator. Int J Biochem Cell Biol 52:26–38. CrossRef Medline

Raike RS, Kordasiewicz HB, Thompson RM, Gomez CM (2007) Dominant-negative suppression of Ca(v)2.1 currents by alpha(1)2.1 truncations requires the conserved interaction domain for beta subunits. Mol Cell Neurosci 34:168–177. CrossRef Medline

Rajakulendran S, Kaski D, Hanna MG (2012) Neuronal P/Q-type calcium channel dysfunction in inherited disorders of the CNS. Nat Rev Neurol 8:86–96. CrossRef Medline

Rose SJ, Kriener LH, Heinzer AK, Fan X, Raike RS, van den Maagdenberg AM, Hess EJ (2014) The first knockin mouse model of episodic ataxia type 2. Exp Neurol 261:553–562. CrossRef Medline

Rotin D, Kumar S (2009) Physiological functions of the HECT family of ubiquitin ligases. Nat Rev Mol Cell Biol 10:398–409. CrossRef Medline

Sakurai T, Hell JW, Woppmann A, Miljanich GP, Catterall WA (1995) Immunochemical identification and differential phosphorylation of alternatively spliced forms of the alpha 1A subunit of brain calcium channels. J Biol Chem 270:21234–21242. CrossRef Medline

Sakurai T, Westenbroek RE, Rettig J, Hell J, Catterall WA (1996) Biochemical properties and subcellular distribution of the BI and rbA isoforms of alpha 1A subunits of brain calcium channels. J Cell Biol 134:511–528. CrossRef Medline

Schwarz LA, Hall BJ, Patrick GN (2010) Activity-dependent ubiquitination of GluA1 mediates a distinct AMPA receptor endocytosis and sorting pathway. J Neurosci 30:16718–16729. CrossRef Medline

Sheng J, He L, Zheng H, Xue L, Luo F, Shin W, Sun T, Kuner T, Yue DT, Wu LG (2012) Calcium-channel number critically influences synaptic strength and plasticity at the active zone. Nat Neurosci 15:998–1006. CrossRef Medline

Soong TW, DeMaria CD, Alvania RS, Zweifel LS, Liang MC, Mittman S, Agnew WS, Yue DT (2002) Systematic identification of splice variants in human P/Q-type channel alpha1(2.1) subunits: implications for current density and Ca2+-dependent inactivation. J Neurosci 22:10142–10152. Medline

Tai HC, Schuman EM (2008) Ubiquitin, the proteasome and protein degradation in neuronal function and dysfunction. Nat Rev Neurosci 9:826–838. CrossRef Medline

Tsai NP (2014) Ubiquitin proteasome system-mediated degradation of synaptic proteins: An update from the postsynaptic side. Biochim Biophys Acta 1843:2838–2842. CrossRef Medline

Vembar SS, Brodsky JL (2008) One step at a time: endoplasmic reticulum-associated degradation. Nat Rev Mol Cell Biol 9:944–957. CrossRef Medline

Veneziano L, Albertosi S, Pesci D, Mantuano E, Frontali M, Jodice C (2011) Dramatically different levels of Cacna1a gene expression between preweaning wild type and leaner mice. J Neurol Sci 305:71–74. CrossRef Medline

Volk S, Wang M, Pickart CM (2005) Chemical and genetic strategies for manipulating polyubiquitin chain structure. Methods Enzymol 399:3–20. CrossRef Medline

Waithe D, Ferron L, Page KM, Chaggar K, Dolphin AC (2011) Beta-subunits promote the expression of Ca(V)2.2 channels by reducing their proteasomal degradation. J Biol Chem 286:9598–9611. CrossRef Medline

Wan J, Mamsa H, Johnston JL, Spriggs EL, Singer HS, Zee DS, Al-Bayati AR, Baloh RW, Jen JC; CINCH Investigators. (2011) Large genomic deletions in CACNA1A cause episodic ataxia type 2. Front Neurol 2:51. CrossRef Medline

Wappl E, Koschak A, Poteser M, Sinnegger MJ, Walter D, Eberhart A, Groschner K, Glossmann H, Kraus RL, Grabner M, Striessnig J (2002) Functional consequences of P/Q-type Ca2+ channel Cav2.1 missense mutations associated with episodic ataxia type 2 and progressive ataxia. J Biol Chem 277:6960–6966. CrossRef Medline

Westenbroek RE, Sakurai T, Elliott EM, Hell JW, Starr TV, Snutch TP, Catterall WA (1995) Immunochemical identification and subcellular distribution of the alpha 1A subunits of brain calcium channels. J Neurosci 15:6403–6418. Medline

Yamada M, Ohnishi J, Ohkawara B, Iemura S, Satoh K, Hyodo-Miura J, Kawachi K, Natsume T, Shibuya H (2006) NARF, an nemo-like kinase (NLK)-associated ring finger protein regulates the ubiquitylation and degradation of T cell factor/lymphoid enhancer factor (TCF/LEF). J Biol Chem 281:20749–20760. CrossRef Medline

Zhou YX, Chen SS, Wu TF, Ding DD, Chen XH, Chen JM, Su ZP, Li B, Chen GL, Xie XS, Dai YF, Wei YX, Du ZW (2012) A novel gene RNF138 expressed in human gliomas and its function in the glioma cell line U251. Anal Cell Pathol (Amst) 35:167–178. CrossRef Medline